RSC Advances

REVIEW

View Article Online
View Journal | View Issue

Cite this: *RSC Adv.*, 2025, **15**, 27668

Catalytic reduction/degradation of methyl orange by metal nanoparticle containing systems: a critical review

Muhammad Arif *

Organic dyes are widely used in many industries, producing health issues after being discharged into wastewater. Methyl orange (MO) is an organic azo dye which is also released into wastewater from different industries and causes toxicity in the environment. Recently, eco-friendly approaches to remove MO from water have garnered significant interest. Among these, the application of inorganic metal nanoparticles (IMNPs) for the catalytic and photocatalytic reduction of MO is an emerging approach for effective and sustainable pollutant remediation. Various IMNPs, which are used for reduction of MO or conversion of MO into eco-friendly products recently through catalytic and photocatalytic reactions, are discussed in this review, as is the synthesis of mono- and bimetallic nanoparticles with and without capping agents which affect their stabilization as well as catalytic performance against MO. The capping agents enhance the catalytic performance of both mono- and bimetallic nanoparticles, recyclable properties, and tuning ability. Additionally, the characterization techniques employed to examine the properties of IMNPs and to monitor the catalytic reduction of MO are discussed. Future research directions should prioritize the separation and characterization of the products formed after MO catalytic treatment to assess their potential applications and improve reaction rates.

Received 9th June 2025
Accepted 29th July 2025

DOI: 10.1039/d5ra04059k

rsc.li/rsc-advances

1. Introduction

Organic dyes are extensively used in various industries, including plastics,[1] cosmetics,[2] leather,[3] textiles,[4] pharmaceuticals,[5] and food[6] production. A large quantity of numerous classes of dyes are generated every year, and approximately 15% of them are discharged into waterbodies through the dyeing procedure, leading to significant health and environmental concerns.[7] The contamination of aquatic resources by these dyes has detrimental effects on the environment and can cause marine diseases such as mucous membrane dermatitis,[8] skin ulceration,[9] hemorrhage,[10] nausea,[11] septal perforation,[12] irritation in the respiratory tract,[13] and cancer.[14]

From various toxic dyes, methyl orange [sodium 4-{[4-(dimethylamino)phenyl]diazenyl}benzene-1-sulfonate] (MO) is an anionic dye with an orange color. MO is an acid azo dye, widely used as an inductor in acid–base titrations as well as dyeing agent in textiles.[15] Use of MO as an indicator is the most common application of it in industries as well as research departments. It indicates the environment of both acidic and basic by various in color.[16] It gives red color in acidic and yellow in basic medium. It is more important than phenolphthalein indicator due to its high differentiating ability between the strong acid and weak base.[17] It also used for adulterant in counterfeit (fake) saffron[18] and cooked foods like Namkeen (salted snacks),[19] tomato ketchup,[20] ice candy,[21] mango shake,[22] and jalebi (Indian sweet),[19] *etc.* Azo group is present in the structure of MO that undergoes anaerobic

Department of Chemistry, School of Science, University of Management and Technology, Lahore 54770, Pakistan. E-mail: Muhammadarif2861@yahoo.com; Muhammadarif@umt.edu.pk

Muhammad Arif

Dr Muhammad Arif is a Professor (Assistant) in Chemistry at Department of Chemistry, University of Management and Technology, Lahore since 2022. He has been working as lecturer in Chemistry at Department of Chemistry, School of Science, University of Management and Technology, Lahore from 2017 to 2022. He has done PhD in Chemistry from University of The Punjab, Lahore, Pakistan. He obtained his MPhil in Chemistry and MSc in Organic Chemistry degrees from Quaid-i-Azam University Islamabad, Islamabad and Institute of Chemistry, University of the Punjab, Lahore, Pakistan respectively. His research area is synthesis, characterization and applications of metal nanoparticles fabricated in microgels and ligands.

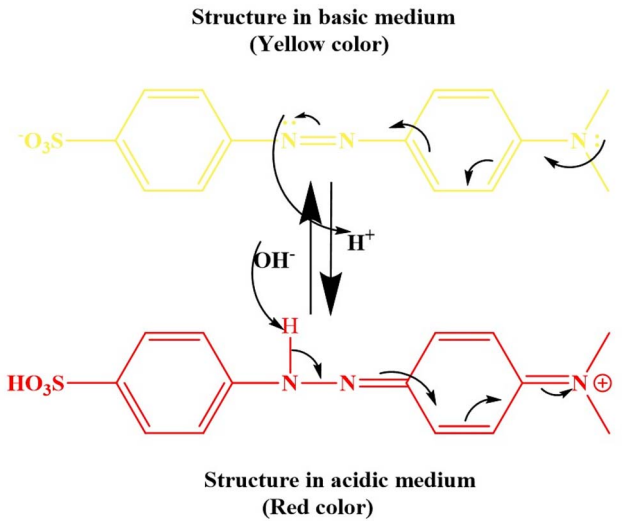

Fig. 1 pH of medium effects on the structure of methyl orange.

degradation through reduction,[23] yielding carcinogenic amines known to cause severe environmental, human, and biological problems.[24] Additionally, it may induce teratogenic impacts on human health. Despite its potential hazards, MO exhibits strong color visibility even at very low concentrations. Hence, it is imperative to reduce MO into non-toxic or less toxic substances before its emission into the natural environment.[25–28] Due to its high chemical and photolytic stability, MO poses challenges in terms of biodegradation owing to its synthetic origin. Various methods have been proposed for the decolorization, detoxification, or treatment of MO dye like catalytic reduction,[29] oxidation,[30] photocatalytic degradation,[31] and adsorption.[32] However, these methods suffer from limitations and drawbacks, primarily concerning energy costs and safety concerns. Major drawbacks include their high cost, inadequacy, rarity of seamless product phase transfer without demolition, and the persistence of pollutant nature post-treatment.

In the adsorption process, the removal of MO from contaminated water through adsorbent leads to the generation of secondary pollutants. Despite gaining considerable attention in current years, photocatalytic degradation of organic dyes faces challenges such as slow reaction rates, severe irradiation environments, and the necessity for high concentrations of photocatalysts, limiting their scalability. From these approaches, the catalytic reduction of MO with IMNPs along with reductant like ($NaBH_4$) has emerged as the most effective approach because of its rapid reduction rate and efficient conversion of contaminated dye in less harmful products.[33–35] Various researchers have explored the catalytic application of bimetallic,[36,37] mono-metallic,[38,39] and tri-metallic[40,41] NPs for both photocatalytic[42–44] and chemical reduction[45,46] of MO. Various review articles have been reported for reduction/degradation of different pollutants[47–49] but no comprehensive review has been published regarding the catalytic treatment of MO dye using various types of metal nanoparticles. This review article highlights those systems which have been used for reduction/degradation of MO in the latest literature.

In this manuscript, Section 1, the introduction, sheds light on the harmful impacts of MO toxicity on both the environment and humans, as well as various methods proposed for its treatment. Section 2 provides insights into the synthesis, origins, and uses of MO across diverse fields. Sections 3 and 4 detail the synthesis of various metal NPs and their integration into several support systems to enhance their stability and catalytic performance, respectively. Section 5 outlines the catalytic processes employed to treat MO dye, aiming to transform it into less harmful and eco-friendly products. Lastly, Section 6 offers an overview of the current status and future directions in MO treatment for green environment.

2. Synthesis and applications of methyl orange

Methyl orange belongs to the family of azo dye. Fig. 1 illustrates the structure of MO that contains two aromatic rings which are connected on both sides of the azo group. One ring contains electron-donating dimethyl amino and electron-withdrawing

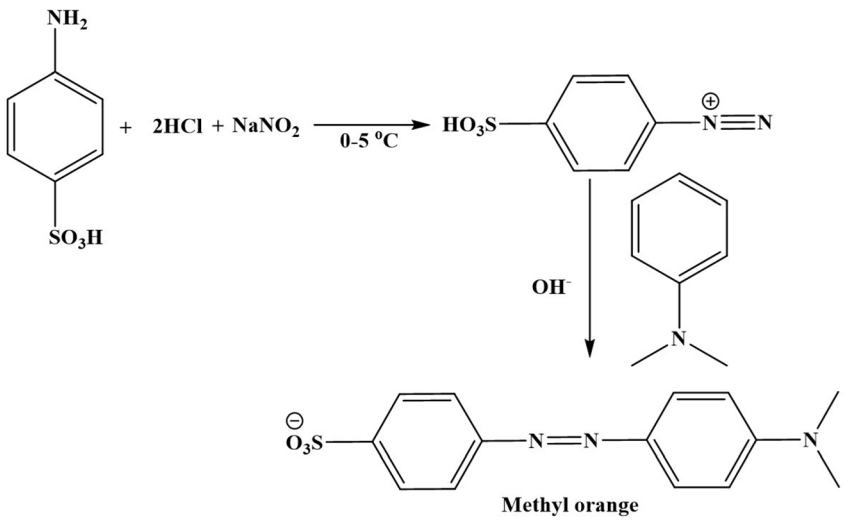

Scheme 1 Synthesis of methyl orange.

sulphonic groups is attached to the other ring. This attachment of electron withdrawing and electron donating groups facilitates decreases the energy gap between highest occupied molecular orbital and lowest unoccupied molecular orbital due to resonance.[50,51] This ability also enhances their stability in the environment.[52] MO finds a wide range of applications due to their photo-physical[53] properties and photostable nature.

Among the various azo dyes, MO stands out as the most commonly used dye in this family, exhibiting remarkable sensitivity to pH[54] and solvent polarity.[55] In acidic conditions, the nitrogen of the azo group of MO becomes protonated, resulting in a cationic form which is indicated by showing red as shown in Fig. 1. Conversely, in basic environments, the protonated nitrogen of azo group is deprotonated, leading to the molecule behaving as an anion with negative charged sulphonate group. This shift is indicated by variation in color from red to yellow. This structural effect of MO can be affected by variation in solvent because each solvent has specific impact on the lifespan and quantum yields anionic and cationic form due to interactions abilities.[56,57] Observations reveal low quantum yield and lifetime of MO lactones owing to electron transfer reactions in excited state. Consequently, both singlet and triplet states of the dye in anionic form are observable. MO finds extensive use as indicator for acid–base titration as well as serving as a colorant in the textile and food industries. This behavior is the most common in the protonated solvents. The synthesis of MO involves two step reaction processes as given in Scheme 1. Initially, 4-diazobenzene sulphonic acid is prepared from 4-aminobenzene sulphonic acid by diazotization in acidic medium at low temperature (0–5 °C). *N*,*N*-Dimethyl aniline attacks the nitrogen of diazonium ion of 4-diazonium benzene sulphonic acid from ring side in basic medium.[58]

3. Reduction of MO with nano-catalyst

Various systems of metal nanoparticles are used as catalysts for reduction of methyl orange as given below.

3.1. Single metal containing nanoparticles

Various metal nanoparticles like Pt,[59] Pd,[60] Au,[61,62] Co,[63] Ag,[64] ZnO,[65] MgO,[66] Fe_3O_4,[67] Co_3O_4,[68] and CeO_2 (ref. 69) have been applied as catalysts for the MO reduction/degradation. These particles have garnered significant attention due to their small size and large surface area, which enhance their catalytic activity. The synthesis of these particles involves the transformation of metal precursor salts through various methods such as microwave irradiation,[70] ultrasonication,[71] hydrothermal,[72] physical,[73] biosynthesis,[74] and chemical methods.

In the chemical method, various reducing agents like $NaBH_4$,[75] polyacrylonitrile,[76] sodium citrate,[77] ascorbic acid,[78] oleylamine,[79,80] hydroxylamine (NH_2OH),[81] and hydrazine hydrate[82,83] are utilized to reduce metal ions into corresponding metal atoms, which subsequently aggregate to form metal nanoparticles (MNPs). Additionally, hexamine is a novel low-cost chemical reducing agent which has also been applied for the MNPs synthesis like Ag NPs from the salts of precursor.[84,85] However, biogenic synthesis of nanoparticles is gaining more attention due to their simplicity, environmental friendliness, and cost-effectiveness.[86] Nevertheless, this method sometimes yields a lesser quantity of NPs. In biogenic synthesis, biological extracts derived from various sources like plants,[87] fungi,[88] algae,[89] and bacteria[90] are employed as a reducing as well as stabilizing agents. They convert the metal ions into their corresponding metal atoms, leading to the formation of MNPs as illustrated in Fig. 2. Various solvent media, including alcohol, water, or mixtures of alcohol and water, are employed for biological extraction of compounds. The biologically extracted products are notably rich in polyphenols and flavonoids.[91] The hydroxyl (–OH) groups of the extracted products serve as reductants, converting metal ions into their corresponding metal atoms. Subsequently, they themselves undergo conversion into carbonyl (–CO–) groups, which in turn stabilize the MNPs through electron acceptor–donor linkage. Additionally, the preparation of metal nanoparticles is achieved through microwave irradiation of solution of precursor salts in the presence of a capping agent in controlled reaction performance[92] as illustrated in Fig. 3. This approach eliminates the need for chemicals which are used as reductants. However, in some cases, chemical reductants are utilized in conjunction with microwave irradiation to ensure an adequate yield of nanoparticles.[93] In this method, the microwave radiation is acted as an electron supplier and converts the metal ions into neutral atomic forms. The metal nanoparticles can also be

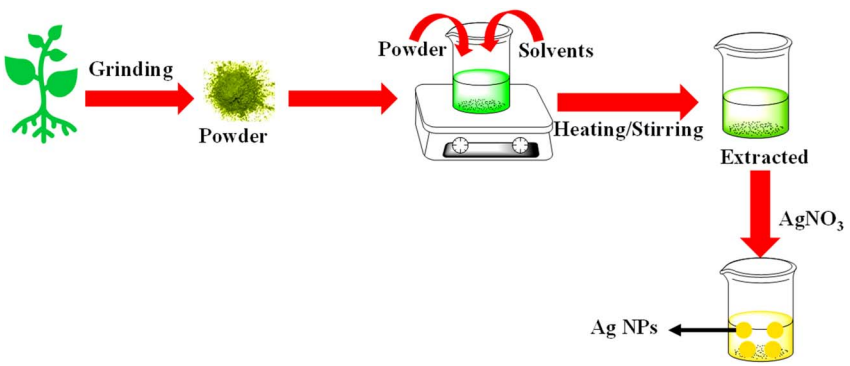

Fig. 2 Synthesis of silver nanoparticles with the help of plant extract.

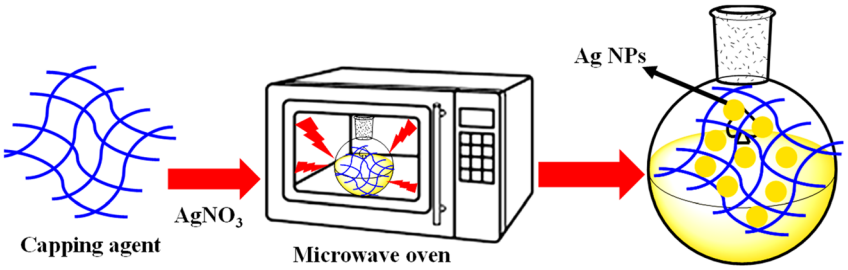

Fig. 3 Silver nanoparticles synthesis by microwave irradiation along with capping agent.

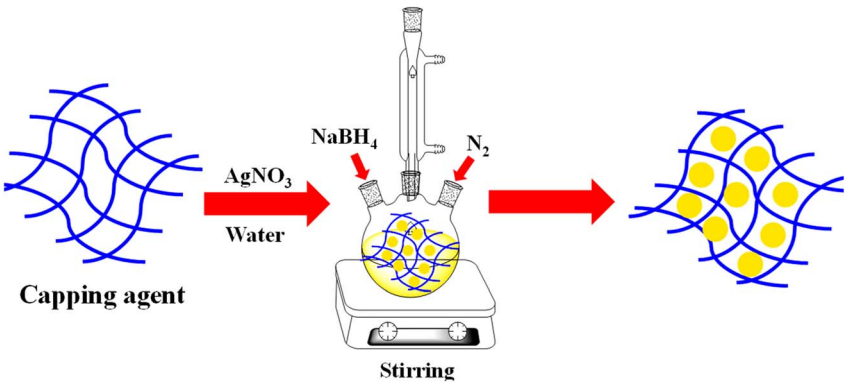

Fig. 4 Synthesis of silver nanoparticles in microgels by *in situ* reduction method.

synthesized by *in situ* reduction method as shown in Fig. 4. The size of synthesized metal nanoparticles is the main issue during these synthetic methods. This issue can be resolved by using a caping agent during the synthesis of metal nanoparticles. In this way, the capping agent can also be used to control the size and stability of metal nanoparticles. Solution of metal salt is added into the dispersion of capping agent. The polar parts of the capping agent attract the metal cations. After insertion of metal cations, $NaBH_4$ solution (freshly prepared) was added which reduced the metal cations into neutral metal atoms. These atoms start to coagulate to form a cluster in nano-range.

Among the various types of metal nanoparticles reported, silver nanoparticles (Ag NPs) are valued for their catalytic capabilities, high electrical conductivity, antimicrobial properties, and cost-effectiveness.[94,95] Ag NPs exhibit significant catalytic efficiency in a variety of pharmaceutical and chemical reactions, making them highly sought-after in various industries.

Gold nanoparticles (Au NPs) are utilized as catalysts in various catalytic reactions of MO. The Au NPs possess distinctive optical and electrical properties along with outstanding chemical reactivity, implementation flexibility, and non-toxic behavior.[96,97] In addition to their catalytic role is present in the applications of pharmaceuticals, electrochemistry, and visual sensing.[98,99] The synthesis of these NPs allows for the attainment of tailored properties, as their efficiency is greatly influenced by factors such as concentration, surface area, shape, and size. Au NPs' catalytic properties render them suitable for MO degradation. They can be synthesized through various methods, including biological, chemical, and physical approaches. However, the biological approach is primarily practiced at the laboratory scale rather than on an industrial scale due to low particle yield and limited understanding of the factors affecting nanoparticle properties. In this method, various microorganisms such as fungi, algae, yeast, and bacteria have been utilized for the Au NP synthesis.

Researchers have additionally documented the production of active Au NPs through the utilization of various metal-tolerant fungi.[100] However, the choice of an appropriate microbial species is crucial for synthesizing nanoparticles with well-defined crystallinity, shape, size, and an enhanced synthesis rate. It is observed that the biochemical performances of microorganisms can be impacted by high metal stress. From these, fungi are particularly employed for extracellular nanoparticle synthesis through secreting a diverse range of metabolites that are large and flexible.

The utilization of plant extracts to induce the synthesis of metal nanoparticles (MNPs) through a green approach has gained widespread acceptance because of the easy plant components availability and ease of the processing.[101,102] Au NPs have been engineered with appropriate functionalizing agents (like L-asparagine).[103] The functionalities of plant extracted material are very important for stability, preventing agglomeration and enhancing lifespan of Au NPs. Additionally, the Au NPs synthesis *via* the chemical method has been reported using a suitable reducing agent like sodium borohydride. However, this method involves the use of chemicals, resulting in minimal cytotoxic effects. Despite the higher cost of precursor salts required for the preparation of Au NPs compared to Ag NPs, it has been noted that the catalytic performance of Au NPs is

generally superior to that of reported Ag NPs in various catalytic reactions.[104]

Ni nanoparticles have been effectively synthesized and employed in catalytic reactions involving MO.[105] However, Ni nanoparticles suffer from significant drawbacks, notably their rapid conversion into oxides, which renders the nanoparticle surface inactive. To enhance the performance of Ni nanoparticles, they are combined with noble metals like Pd, Pt, Au, or Ag to produce bimetallic NPs (Ni_xX_y).[106] Consequently, these nanoparticles demonstrate synergistic properties derived from both types of nanoparticles.

Seku and his coworkers[107] described a simple method for synthesizing Ag NPs using microwave-assisted irradiation in water, employing green chemicals like *Frankincense* gum as a reducing agent as well as a stabilizer. This method has garnered significant attention recently due to its adherence to three key principles of green nanoparticle synthesis: the use of a non-toxic reductant, a reusable and cheap stabilizer, and an environmentally safe solvent system. Furthermore, this approach offers several appealing characteristics, including a lower energy consumption, short reaction time, and improved product yield. The irradiation of microwave creates homogeneous growth and nucleation conditions for NPs by rapidly and uniformly heating the medium of reaction. The authors noted that the absorbance peak at 425 nm began to rise after a few mins of reaction proceeding and became more significant after some time. The color of dispersion changed to a yellowish-brown hue, confirming the Ag NP formation. The sample was scanned in UV-visible spectrophotometer over a few months. The results showed that the position and intensity of the surface plasmon resonance (SPR) band remained consistent, indicating the highly stable NP formation. They examined that the hydroxyl groups of *Frankincense* stabilize the Ag NPs and the Ag ion reduction, albeit to a limited extent. Consequently, the hydroxyl groups of *Frankincense* attract the Ag^+ ions because of electrostatic attraction. Hydroxyl groups of *Frankincense* under microwave irradiation contribute to the reduction of these silver ions. Subsequently, these reduced silver starts to nucleate, facilitating the formation of nano-sized clusters (7 ± 2) of MNPs. Furthermore, the –OH groups encapsulate the nanoparticles, preventing their agglomeration. They used these nanoparticles for reduction of MO, RhB, and MR as well as antibacterial activity against *Escherichia coli* (*E. Coli*), *Bacillus series* (*B. Series*), *Bacillus subtilis* (*B. Subtilis*), and *Pseudomonas aeruginosa* (*P. Aeruginosa*).

Naseem *et al.*[108] synthesized Ag nanoparticles with *in situ* reduction in the presence of sodium dodecyl sulfate (SDS) as stabilizer. The SPR peak appeared at 410 nm in UV-visible spectrophotometer. They were employed these for MO degradation along with $NaBH_4$. Numerous other researchers have also reported the synthesis of mono-metallic NPs using various methods for treating MO.[109–112]

Monometallic systems show moderate activity but are often outperformed by bimetallic or trimetallic counterparts due to synergistic effects. Here is only one atom in the cluster of nanoparticles with show catalytic activity. The electron transferring capacity of monometallic systems is not better than bi-metallic and tri-metallic nanoparticles.

3.2. Bimetallic nanoparticles

The nanoparticles which contain two different metals are called bimetallic nanoparticles. Au–Ag,[104] Au–CeO,[113] Au–Cu_2O,[81] Pd–Au,[114] Ag–Cu,[115] Cu_2O–Ag,[116] Ag–Co,[117] AgO–NiO,[118] Au–Fe_3O_4,[119] Au–Co,[120] Ni–Ag,[121] Fe–CdO,[122] Pd–Rh,[123] Mn–Cu,[124] and PdO–NiO[125] are the examples of bimetallic nanoparticles which are used as catalysts for MO reduction. A review on bimetallic nanoparticles loaded in microgels has been reported by me.[126] The bimetallic systems showed better catalytic performance owing to their synergistic effect compared to monometallic nanoparticles. Bimetallic nanoparticles exhibit superior surface properties to individual metallic NPs. These NPs possess different structural architecture, wherein two monometallic alloys are connected to form bimetallic nanoparticles, and their structural arrangement depends on the synthetic conditions, kinetics of reduction, and miscibility metal ions. As a result, these NPs pose multiple structural morphologies than monometallic NPs. It has also been noted that their surface plasmon band energy, selectivity, catalytic activity, morphological composition, and magnetic properties differ from those of individual metal nanoparticles. Various strategies are employed for the preparation of bimetallic NPs like photolytic reduction, green synthesis using biological extracts, solvothermal approaches, sonochemical methods, solvent extraction–reduction, borohydride reduction, polyol processes, and seed growth method.[43,127–129] Bimetallic nanoparticles exhibit superior catalytic efficiency through the combination of different metal nanoparticles. One of the key advantages of bimetallic nanoparticles is their synergistic properties, incorporating both nanoparticles and distinctive electronic effects, which contribute to their high catalytic activity.

Minal and his coworker[130] explained the synthesis of bimetallic (Ag/Pd) nanomaterials using a green approach, wherein leaves of *Citrus limon* served as reductant as well as structural controlling agents. During bimetallic NP formation, both Ag^+ and Pd^{2+} ions (produced from their corresponding precursor salts) interacted with polar functional groups to form complexes. Produced complexes were subsequently reduced slowly to Ag and Pd atoms by extracted materials (carboxylic groups containing compounds). The reduction of metal ions led to the development of metal nuclei through homogeneous nucleation to obtain stability. The atomic nuclei then underwent processes such as Ostwald ripening, orientation, growth, and crystal fusion under the influence of compounds present in the *Citrus limon*, resulting in the production of bimetallic (Ag/Pd) nanoparticles.

Singaravelan and colleagues[131] employed the electrochemical method to prepare both monometallic and bimetallic (Zn/Cu) NPs, utilizing metal salts as precursors of corresponding metal ions. Cu is less reactive than Zn. Therefore, Cu is deposited on Zn during this method. These nanoparticles were then utilized as active catalysts for the MO degradation. Ghosh and coauthors[132] reported the synthesis of bimetallic (Ag/Au)

nanoparticles. They used the extracted material of leaves of *Polyalthia longifolia* as reductant and controlling the size of NPs. They degrade different dyes along with MO.

Bimetallic systems of nanoparticles are better than monometallic systems because these systems have synergistic effect. This effect facilitates transferring the electron from reductant to MO during catalytic performance. But their structural elucidation is a main task for bimetallic systems like their morphology is core–shell or homogenous distribution of both metals. Their recycling ability reduces catalytic activity as compared to monometallic system due to greater leaching effect of one type of metal nanoparticle due to various particle sizes.

3.3. Tri-metallic nanoparticles

The nanoparticles which have three metals in their morphology are called tri-metallic nanoparticles. They were synthesized using a seed-mediated process and were reported for their effectiveness in the MO reduction. For this synthesis, they employ three dissimilar precursor salts to obtain catalysts exhibiting properties of three distinct types of metal nanoparticles.[42] These nanoparticles demonstrate superior properties compared to bi- and mono-metallic nanoparticles. Riaz *et al.*[133] developed tri-metallic (Fe–Ni–Co) nanoparticles *via* a co-precipitation approach involving single steps. They mixed the salt solutions of all these metals in basic medium and stirred overnight at 50 °C. The precipitated product was centrifuge and then washed (ethanol + water) and calcinated in muffle furnace. These nanoparticles were utilized as catalysts for MO degradation. A schematic representation of the synthesis of tri-metallic nanoparticles is illustrated in Fig. 5.

The catalytic performance of tri-metallic particles is better than mono- and bi-metallic systems due to greater synergistic effect and they more easily transfer the electrons from reductant to pollutant. The catalytic activity of these systems can be further enhanced in composite form ref. 134 and 135. Their structural elucidation is a task for the researchers whether they have core shell morphology or alloy formation. Their catalytic performance rapidly decreases on recycling due to the high leaching effect of metal nanoparticles from these systems. Therefore, the synergistic effect reduces and hence catalytic activity decreases. Their reaction conditions are also greatly affected by these systems as compared to mono- and bi-metallic systems. Because different metals show different behavior under different conditions while this effect is minimal in monometallic systems.

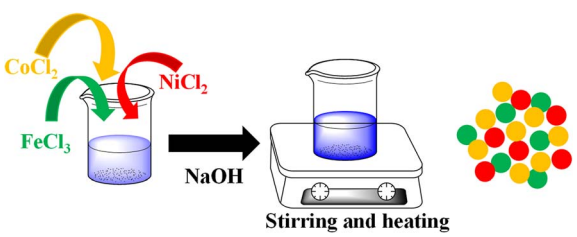

Fig. 5 Fe/Co/Ni tri-metal nanoparticles synthesis.[133]

4. Supporting material

IMNPs are very unstable. They tend to agglomerate and transform into massive products, leading to the loss of their high surface properties. Additionally, their small size makes it challenging to separate them from the reaction mixture, resulting in their wastage during catalysis. To prevent agglomeration, facilitate easy recovery, and maintain stability, various supporting systems have been reported by different scholars.[136–139] Several supporting materials, including polymeric,[140] inorganic,[141,142] zeolites,[143] and organic[26] materials, have been utilized by investigators to successfully fabricate IMNPs.

4.1. Organic/inorganic materials

Various inorganic compounds, including activated carbon, nitrogen-doped carbon nanodots,[144] carbon nitride (CN) sheets,[145] silver colloids,[146] Fe_3O_4,[67] TiO_2,[147] SiO_2,[148] reduced graphene oxide (RGO),[149] graphene oxide (GO),[150] and graphene sheets,[151] have been identified as supporters with fabrication of IMNPs under dissimilar reaction conditions which depend on the desired surface active area of nanomaterials.

Fe_3O_4 particles with nano-scale sizes have garnered significant interest as supporters for noble metal nanoparticles because of their magnetic characteristic, including irreversibility in high field, superparamagnetism, high field saturation, and shifting in loops after cooling of field.[67,152] These characteristics arise during the shifting of electron between Fe^{3+} and Fe^{2+} ions in the sites of octahedral shape, enabling easy recyclability and recovery of the material through the application of an external magnet. Various techniques are employed for Fe_3O_4 NP synthesis like polymer template method, thermal decomposition, polyol-mediated sol–gel, and solid-state method methods. From these methods, co-precipitation is considered as the best synthetic method, involving two different procedures.

- Employing an oxidizing solution facilitates the co-precipitation of partially oxidized Fe^{3+} and Fe^{2+} ions.[153]
- Utilizing a base enables the direct co-precipitation of Fe^{3+} and Fe^{2+} ions.[154]

Fe_3O_4 NPs exhibit some disadvantages, including instability, larger crystallite size, poor stoichiometry, and inhomogeneity, which can cause magnetic nanoparticles to lose their characteristics. This challenge can be resolved by modification of surface of magnetic nanoparticles with organic polymeric networks. This modification can be achieved through various methods like surfactant adsorption, polymer coating, organic-vapor condensation, and direct silanation using a silane coupling substance. Among these methods, the implant of organic polymeric substance onto magnetic nanoparticles is considered the most effective. A polymer network formation round magnetic NPs (core) provides storage stability, non-toxicity, control over chemical composition, malleability, and the introduction of different functionalities on the NP surface for the physical adsorption of different substances. This process alters the properties of the superparamagnetic NPs surface, increasing their biocompatibility (*i.e.*, reducing their toxicity) in aqueous media and preventing particle surface oxidation.

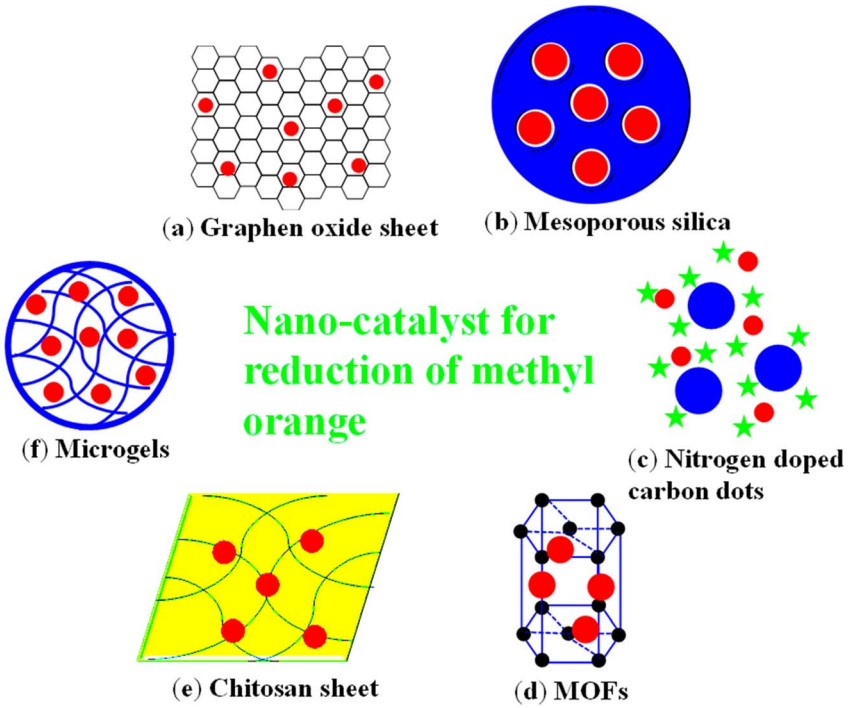

Fig. 6 Metal nanoparticles fabrication with (a) graphene oxide, (b) mesoporous SiO_2, (c) N-doped C dots, (d) metal–organic frameworks, (e) chitosan, and (f) microgels.

The sheets of graphene oxide (GO) represent another class of two-dimensional materials characterized by numerous oxygen-containing functional groups, including carboxylic acid, hydroxyl, and epoxy groups in their structure.[149] These species have great potential for adsorption of aromatic organic dyes because of their strong π interaction, large surface area, aromaticity, and chemical robustness, thereby accelerating the reduction rate of these dyes on the attachment with metal nanoparticles. GO exhibits optical, physicochemical, and intrinsic electronic properties along with fluorescence-quenching capabilities.[155] However, GO often requires modification for various applications. The properties of emission and chemical performance of GO can be enhanced through heteroatom substitution. Nitrogen (N) is particularly favored for chemical doping of C-containing materials due to its strong valence bonds and similar atomic size. N-doped GO (NGO) exhibit higher chemical activity than GO alone.[156] NGO serves as catalyst for hydrogen peroxide (H_2O_2) decomposition, generating hydroxyl radicals which are utilized for oxidation of MO.[157] GO is transformed into reduced graphene oxide (RGO) using various reducing agents like plant extracts, ascorbic acid, or sodium borohydride, which reduce different functional groups of oxygen present in the network of GO with enhancing resonance. This conversion reduces the hydrophilic nature of GO and enhances its conductivity. Consequently, electron transfer from reductant to MO is increased during the degradation with MNPs decorated RGO compared to MNPs decorated GO. The synthesis of MNPs in RGO, GO, and graphene sheets is depicted in Fig. 6(a).

Silica nanoparticles have emerged as efficient supporting materials to the MNPs. Mesoporous silica (MS) possesses a high surface area, large pore size, and a highly organized network.[158] By treating MS with various chemicals, its functional groups can be enhanced, thereby increasing the active sites for fabrication.[159] These features facilitate the maximum loading and widespread distribution of MNPs, resulting in enhanced catalytic performance and stability.[142] A schematic representation of fabrication of MNPs in MS is illustrated in Fig. 6(b). An additional remarkable class of supporting materials is carbon (C) NPs and N-doped CNPs (NCNPs).[160] C dots offer significant surface properties and alleviate the barrier of diffusion of reactants to MNPs surface.[161] N-doping of CNPs effectively modulates their intrinsic behaviors. This process enhances their surface chemical performance, as well as their electronic and optical properties. Consequently, N-doping increases the active sites of the nanoparticles, facilitating approaching the surface of MNPs. A diagrammatic representation of MNPs fabrication with nitrogen-doped CNPs is given in Fig. 6(c). However, MNPs are not easily separated during catalysis due to their small particle size. This challenge can be achieved by modification of magnetite materials like Fe_3O_4 NPs[162,163] along with MNPs. These materials prevent agglomeration of the nanoparticles and enable their recovery after catalysis. Their magnetic properties make them perfect for catalysis due to ease recycling property simply by applying a magnetic field.

Activated carbon (AC) has been identified as an effective stabilizer for the synthesis of metal nanoparticles.[164] Derived from the pyrolysis of various plant materials like soybean hulls, sugarcane bagasse, coconut shells, and bagasse, AC is obtained through a pyrolysis process in muffle furnace in inert atmosphere and high temperatures (approximately 800 °C), resulting in powdered C. Subsequently, its efficiency is enhanced by

treating acidic media, yielding functional AC with higher density. AC provides a large surface area for fabrication with MNPs, which in turn exhibit high catalytic performance for MO.[165]

Alotaibi *et al.*[150] conducted a study on the synthesis of gold (Au) NPs on the surface of graphene oxide (GO) in the absence of reducing agents. They used hydrogen molecules which were obtained by splitting water through applying UV irradiation. They degraded the MO and MB dyes from water using H_2O_2. Boukoussa and his coworkers[164] synthesized different nanoparticles along with activated carbon (AC) by using $NaBH_4$. They synthesized Cu NPs (Cu–AC composite), Ag NPs (Ag–AC composite) and Fe NPs (Fe–AC composite) along with AC and then used these systems for catalytic reduction of MO, 4-nitrophenol (4NP), and MB along with $NaBH_4$. Among these composites, Cu–AC showed greater catalytic activity than Fe–AC and Ag–AC due to better dispersity of Cu NPs on AC surface. Obtained reduction rate were 0.0259 s^{-1} for MB, 0.0218 s^{-1} for MO, and 0.0074 s^{-1} for 4NP. Bagherzadeh *et al.*[148] have reported the synthesis of Ag NPs containing SiO_2 by γ-irradiations. They reduced MB, Congo red (CR), and MB dyes from water. They used $NaBH_4$ during these catalytic reduction reactions. Vu *et al.*[141] studied the synthesis of composites of Ag NPs and Fe_3O_4 by hydrothermal process. They applied this composite system against 4NP and MO reduction.

Easy recycling ability of this composite system (Fe_3O_4-MNPs) dominates over the other systems due to magnetic properties. The leaching of metal nanoparticles is also controlled by these systems. But the high porosity and interactions with pollutants are present in AC-MNPs, SiO_2-MNPs, and GO-MNPs.

4.2. Metal–organic framework (MOF)

In these systems, organic components are linked with metal ions with coordinate covalent bonds to form long chain products. MOFs have garnered considerable interest among investigators for their intriguing role as stabilizers in the fabrication of magnetic nanoparticles due to their high porosity.[166] MOFs are 3D structures that are very suitable matrices with distinct functionalities which make them perfect for specific applications. Generally, they are composed of metal cations and carboxylic groups containing aromatic ligand. These groups make them excellent support materials for MNPs. MOFs offer advantages such as ensuring the longevity of nano-catalysts, enhancing their performance, and expanding the range of reactions they can catalyze by providing the necessary components that may be lacking.[167] MOFs have also been utilized as precursors for the synthesis of magnetic nanoparticles as well as catalysts for MO reduction. These composites exhibit unique structural arrangement, allowing for the creation of well-designed porous frameworks with specific pore shapes, sizes, compositions, and adjustable functionalities to facilitate the expansion and detention of MNPs as needed.[168,169] Three distinct approaches are employed for production of MNPs using MOFs as supporting materials: constructing MOFs around pre-existing MNPs, loading MNPs onto the surface of MOF pores, or embedding MNPs within the nanopores of MOFs. This integration of MNPs with MOFs not only leads to functional synergy but also enhances their individual strengths while mitigating drawbacks. The configuration of MNPs loaded onto MOFs is depicted in Fig. 6(d).

Currently, a subgroup of MOFs known as zeolitic imidazolate frameworks (ZIMFs) has been employed as a support for MNPs fabrication.[170] ZIMFs are characterized by the presence of imidazole-based ligands along with transition metal cation, resulting in materials with crystalline topology. Above 150 ZIMF systems have been successfully synthesized. These networks exhibit exceptional chemical and thermal stability due to their specific surface, tunable pore apertures, and microporous configurational properties.[123]

Karimi *et al.*[171] described the synthesis of a three-dimensional MOF loaded with Pd NPs and Au NPs, which was then used for MB, MO, MR, 2NP, 3NP, and 4NP reduction as well as Sonogashira–Hagihara alkynylation coupling. The catalytic performance of these systems was also observed under different solvents. High yield of products was obtained in high polar solvents as compared to low polar solvents. This is perhaps the highest solubility effect in high polar solvents. It also reported that the yield of those products was high which have electron-withdrawing groups in their structure. In this case, the shifting of electrons from metal nanoparticle surface to reductant increases if the electron-withdrawing group is attached with their structure.

4.3. Polymeric material

Various polymeric materials like microgels[96,117,172,173] and hydrogels[140,174,175] with various compositions and morphology, natural polymers (alginate,[176] cyclodextrin,[177] poly(dopamine) (PDA),[178] cellulose,[179] and chitosan[180]) and synthetic polymers (poly(*N*-isopropylacrylamide) [P(NIPAM)],[181] dendrimers,[182] polyvinylpyrrolidone (PVP),[183] poly(ethylene glycol) [P(EG)],[184] poly(*N*-isopropylmethacrylamide) [P(NIPMAM)],[185] and poly(-vinyl alcohol) [P(VA)][138]) have been reported as supporting agents for the fabrication of MNPs. Chitosan (polysaccharide of biological origin) has also been employed as supporter for fabrication of MNPs,[75] as illustrated in Fig. 6(e).

Some of these materials have been identified as surface capping agents capable of controlling the shape and size of MNPs.[181,186,187] However, their use as surface capping agents is limited due to strong interactions between MNPs and different functional groups, which can block catalytically active sites and lead to reduce the catalytic activity. To tackle this limitation, investigators have developed porous polymer materials to serve as support for nanoparticle immobilization.[26] Porous materials offer the advantage of creating specific surfactant-free active sites and controlling nucleation, thereby reducing particle aggregation and maintaining them in nano-sized regimes. For these porous materials, long polymer chains are particularly effective for supporting and stabilizing nanoparticles because of unique structural network. However, there is a risk of many MNPs leaking out or detaching from the polymer surface upon direct exposure to the medium, potentially compromising the catalytic activity of the composite material.

From these, dopamine (DA) has emerged as a suitable candidate for fabrication of MNPs.[188,189] DA is a small organic molecule mimicking mussel-foot-proteins and serves as a crucial neurotransmitter in the brain. DA contains amine and catechol in their structure and can perform self-polymerization in basic medium to form polydopamine (PDA). The microparticles of PDA are easily synthesized at ambient temperature. Studies have shown that PDA is hydrophilic, non-toxic, and environmentally friendly along with safe biocompatibility. PDA with o-quinone/catechol is readily synthesized at ambient temperature. Their size varies based on the environments of reaction like solvent, temperature, initial DA concentration, and pH. PDA-decorated nanomaterials have been utilized for MO reduction. PDA acts as a redox mediator (RM), facilitating the decolorization of MO by $NaBH_4$. RMs show reversible reduction/oxidation reactions which enhance the reduction rate of dye. Moreover, they can serve as electron carriers in multiple redox reactions, lowering the activation energy (E_a) of the reaction.[189]

Others (hydrogels, nanogels, microgels, and dendrimers) have been synthesized using methods such as precipitation polymerization,[117] dispersion polymerization,[190] and inverse microemulsion polymerization.[191] These particles possess a sieve-like shape that readily incorporates MNPs and retains them for extended periods, ensuring stability. Additionally, they show responses to external stimuli such as ionic strength, pH, and temperature, allowing them to adjust their size and, consequently, the size of MNPs. The size of the polymer particles' sieves is controlled by adjusting the contents of monomers, comonomers, and crosslinker during synthesis. Therefore, polymers decorated with MNPs exhibit synergistic properties, combining the swelling/shrinking behavior of polymers with the surface-based catalytic behavior of MNPs.[181]

From these materials of polymers, dendrimers have branched into their polymeric network and MNPs are simply fabricated on their surface at specific reaction conditions.[176,192,193] From these systems, NPs have the maximum chance of leaching in the reaction medium and not recycled easily. However, these systems have less diffusion barrier for MO to reach the MNP surface, reducing the time required for the reduction. In hydrogels, nanogels, and microgels, many MNPs are inserted in the sieves. The loading of MNPs in the sieves prevents them from leaching into the reaction medium. Nevertheless, it creates a large diffusion barrier for MO molecules to reach the surface of MNPs and hence reduce the rate of reduction and prolong the reaction time.[117]

Arif[121] have synthesized bimetallic (Ni/Ag) nanoparticles containing poly(*N*-isopropylmethacrylamide-methacrylic acid) Ni/Ag–P(NIPMAM-MAA) Ni/Ag–P(NM) hybrid microgels and used it for catalytic reduction of different azo dyes from water. The temperature and pH effect on swelling and deswelling behavior of these hybrid systems were also investigated. The system was present in swelling state at basic medium and deswelling in acidic conditions. Similarly, temperature of medium was also impact on the swelling/deswelling behavior of Ni/Ag–P(NM). The reduction rate of MO depends upon the content of $NaBH_4$, MO, and Ni/Ag–P(NM) dose.

Bawazeer[33] studied the synthesis of Fe nanoparticles decorated polyacrylate (Fe-PAL). Degradation studied of MO was investigated under different conditions of temperature and pH of medium. The degradation rate of MO increased by increasing the temperature, pH, and Fe-PAL dose.

Numerous other researchers have utilized microgels and hydrogels to fabricate and stabilize MNPs, extending their longevity.[181,185,194,195] The microgel network integrated with MNPs is depicted in Fig. 6(f).

5. Catalytic treatment with methyl orange

MO dye has been treated with various metallic systems through different methods like photocatalytic degradation, reduction, and oxidation with employing light, reducing agent and oxidizing agent respectively. These processes are outlined below.

5.1. Reduction method

In chemical reduction methods, the MNPs along with a reducing agent are employed to treat harmful pollutants like MO.[34] In an aqueous solution, MO exhibits a strong absorption peak (λ_{max}) at 464 nm in the UV-visible spectrum. $NaBH_4$ (reducing agent) converts MO into leuco MO molecules, which subsequently degrade into less toxic substances. However, this method is time-consuming, produces toxicity (by excess amount of $NaBH_4$), and therefore impractical. A nano-catalyst reduces the barrier of energy by lowering the E_a, thus expediting the reaction. Noble metal nanoparticles serve as catalysts,[196] garnering significant attention due to their distinctive physical and optical properties, rendering them suitable for various catalytic applications. Their high reactivity is attributed to their large surface-to-volume ratio,[34] which accelerates the reduction of dye molecules into non-toxic substances by reducing the kinetic energy (KE) required for electron transfer.[33]

Investigators have noted that the catalytic reduction of MO conforms to a pseudo-first-order kinetic model, primarily owing to the abundant use of the reductant ($NaBH_4$).[36] The reaction rate is solely dependent on MO concentration,[197] thus making it a first-order reaction concerning the MO concentration. According to a first-order model, the representation of rate for this reaction is represented by eqn (1).

$$\text{Rate of reduction} \propto [\text{MO}] \tag{1}$$

$$-\frac{dC_t}{dt} \propto C_t \tag{2}$$

$$-\frac{dC_t}{dt} = kC_t \tag{3}$$

By rearranging eqn (3) as

$$-\frac{dC_t}{C_t} = k\,dt \tag{4}$$

Integrating both sides of eqn (4)

$$-\int \frac{dC_t}{C_t} = k\int dt \quad (5)$$

$$-\ln C_t = kt + C \quad (6)$$

At initial condition of reaction, when $t = 0$ then $C_t = C_o$, so eqn (6) becomes

$$-\ln C_o = C \quad (7)$$

Putting eqn (7) in eqn (6) as

$$-\ln C_t = kt - \ln C_o \quad (8)$$

Rearranging eqn (8) as

$$\ln C_t - \ln C_o = -kt \quad (9)$$

$$\ln \frac{C_t}{C_o} = -kt \quad (10)$$

Here, C_t represents the MO concentration at any given time (t), C_o stands for initial MO concentration, t stands for reaction time, and k represents a constant. Another representation of eqn (10) in terms of absorbance (A) according to Beer's Lambert law is shown below:

$$\ln \frac{A_t}{A_o} = -kt \quad (11)$$

In eqn (11), A_t represents the value of absorbance for MO at any time (t), A_o stands for initial absorbance, t represents the reaction time, and k denotes the rate constant. The value of k is determined from the slope value of the plot between time and $\ln(C_t/C_o)$. As the reaction of reduction progresses, the MO concentration decreases gradually, leading to a decrease in absorbance as well. The k for the MO reduction is also influenced by some other factors like the temperature, pH, concentration of MO, amount and nature of the catalyst used in the reaction.

The catalytic reduction mechanism of MO with reductant ($NaBH_4$) and MNPs composites is depicted in Fig. 7. It has been observed that the MO reduction follows both the Eley Ridel (ER) mechanism and the Langmuir Hinshelwood (LH) mechanism during the catalytic reduction. Initially, the reactant molecules diffuse to the MNP surface, where they adsorb and react to form the product. The adsorbed product then desorbs and diffuses out according to the LH mechanism. While one of the reactant molecules adsorbs onto the catalyst surface and reacts with the unadsorbed reactant to produce the product in the ER mechanism. Products then desorb and diffuse to the reaction medium (bulk), making the active sites accessible for remaining reactant molecules.

5.1.1. Electrons transfer mechanism. When the catalytic reduction of pollutants is performed in the presence of both catalyst and reductant ($NaBH_4$). In this process, $NaBH_4$ initially dissociates into BH_4^- ions. These ions are then electrostatically adsorbed onto the catalyst surface.[181] Upon adsorption, the borohydride ions further converted into hydrogen (H) atoms, releasing electrons that are transferred to the surface of catalyst. The catalyst serves as an electron relay system, facilitating the transfer of electrons from BH_4^- (donor) to MO (acceptor).[121]

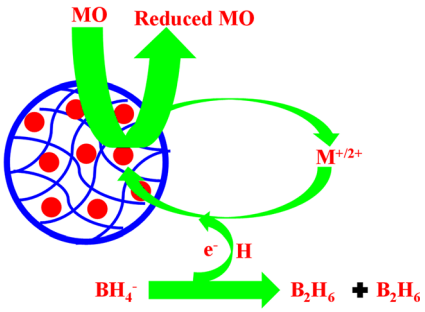

Fig. 7 Catalytic reduction mechanism of methyl orange in the presence of $NaBH_4$ and metallic nanocatalyst in capping agent.

5.1.2. Method of MO interaction with H atom. A hydrogen atom (after electron transfer) originating from the borohydride (BH_4^-) ions reacts with a neighboring MO molecule, resulting in the simultaneous hydrogenation of MO due to electron transfer. Electrons are transferred from the surface of catalyst to the MO (acceptor) molecules, converting them to its reduced form (leuco MO) (LMO).[198] This process involves the cleavage of the double bond of azo (–N=N–) group (chromophoric component) of the MO molecule, leading to a change in the solution's color.[199]

Arif *et al.*[117] described the synthesis of bimetallic (Co/Ag) nanoparticles in poly(*N*-isopropylmethacrylamide) to form Co/Ag–P(NIPMAM) hybrid system. They investigated catalytic behavior against MO in the presence of $NaBH_4$. They obtained 0.48 min^{-1} value of apparent rate constant (k) during the reduction of MO. The researchers elucidated the mechanism underlying the MO reduction with catalyst through several steps. Initially, both MO and BH_4^- ions (produced from reductant ($NaBH_4$)) co-adsorb onto the Co/Ag nanoparticle (catalyst) surface. Both reactants can easily adsorb/desorb from the surface of nano-catalyst. Molecules of MO were quickly adsorbed onto the Co/Ag surface owing to the interaction between the MO and Co/Ag. During reduction, electrons are transported from BH_4^- (reductant) ions directly to the Co/Ag NPs through P(NIPMAM). The functional groups present on the surface of P(NIPMAM) help in this sifting of electrons from BH_4^- ion to MNPs. Subsequently, these electrons are shifted from the surface of nano-catalyst to MO to reduce them into non-toxic products. The catalyst demonstrated excellent recyclability, maintaining activity for up to five cycles, and remarkable efficacy in treating wastewater contaminated with dyes. Various other researchers have also investigated different nanocatalysts for the chemical reduction of MO using $NaBH_4$.[200–203]

5.2. Photocatalytic degradation of MO

Photo-catalysis presents an intriguing approach for addressing MO molecules.[204] Numerous studies have explored the

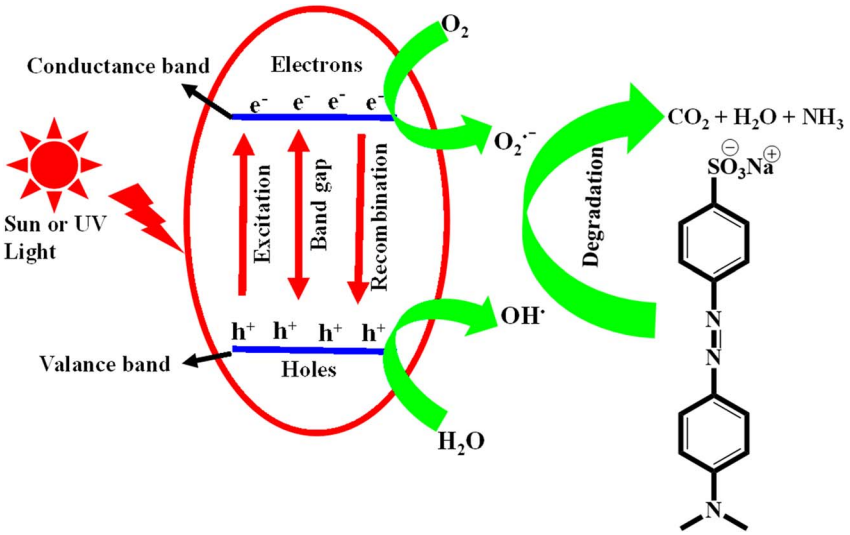

Fig. 8 Photocatalytic degradation mechanism of methyl orange.

photocatalytic capabilities of various catalysts for MO degradation under solar light or UV exposure[205–208] as illustrated in Fig. 8. Mechanistically, it is now widely accepted that the dye serves as the primary light-absorbing species.[209] The photocatalytic degradation has more advantage than chemical methods, as it avoids secondary pollutants to the ecosystem. Many scholars have investigated the application of various types of nanoparticles (like TiO_2 (ref. 210)) for the photocatalytic MO degradation under various reaction conditions, including catalyst concentration, radiation intensity, and irradiation duration.

Thi Thu Nhu and Nguyen[204] investigated the photocatalytic degradation of MO using Ag doped TiO_2 nanoparticles. This system was synthesized by gamma irradiations. The percentage of Ag^+ ions during each synthesis used ratio by weight was different. The system with 1% wt of Pt doped TiO_2 showed excellent photocatalytic activity as compared to other ratios due to high porosity and lowest band gap. They also investigated the catalytic performance under different pH, dye concentration, and content of doped material. Pt doped TiO_2 also exhibits better recycling ability after photocatalytic degradation of MO. The kinetic study revealed that the degradation process followed a pseudo-first-order model.[16] Other investigators have reported the utilization of various nano-catalysts for treating MO.[139,146,211–213] This approach aims to avoid the use of toxic and harsh reaction conditions.

5.3. Oxidative approach of MO

MO degradation can also be achieved through oxidation, where the dye is converted into harmless products with nano-catalysts and oxidant.[214] In aqueous medium, MO dye exists in the form of anions. Transition metal oxides are used as catalysts to accelerate the oxidation of MO into harmless components, leveraging their different crystallinity and surface area properties. Wet air oxidation (WAO) stands out as one of the most effective and easy methods for oxidizing organic pollutants like MO. This method involves generating active oxygen species (hydroxyl radicals) at high pressures and temperatures.[215] The oxidation of MO through WAO produces products such as *N*,*N*-dimethyl-*p*-phenylenediamine, sulfanilic acid, benzenesulfonic acid, *N*,*N*-dimethylbenzenenamine, and benzenesulfonic acid, which are initially harmful to the environment but eventually break down into lower molecular weight acids and, ultimately, into CO_2, NH_3, and H_2O (final products).[42] Fenton-like oxidation is another effective and environmentally friendly method for MO degradation.[73] Fe/Cr quantum dot-doped mesoporous silica and then composite with activated carbon have been identified as a nano-catalyst for the oxidative degradation of MO. Fenton-like oxidation can be heterogeneous or homogeneous. Heterogeneous approach is particularly effective at neutral (usually 7) pH and prohibits the Fe sludge formation. In the homogeneous approach, hydroxyl radicals (OH) are generated through H_2O_2 and Fe^{2+} reaction, converting MO into non-toxic substances. The mechanism developed by homogenous approach is depicted below (eqn (12)–(16)).

$$Fe^{2+} + H_2O_2 \rightarrow Fe^{3+} + \dot{O}H + OH^- \quad (12)$$

$$Fe^{3+} + H_2O_2 \rightarrow Fe^{2+} + \dot{H}O_2 + H^+ \quad (13)$$

$$Fe^{2+} + \dot{O}H \rightarrow Fe^{3+} + OH^- \quad (14)$$

$$\dot{O}H + H_2O_2 \rightarrow \dot{O}H_2 + H_2O \quad (15)$$

$$\dot{O}H + \dot{H}O_2 \rightarrow H_2O_2 + O_2 \quad (16)$$

Some limitations restrict the efficiency of homogeneous Fenton reactions, including the low utilization of H_2O_2, the requirement for harsh pH conditions, the production of iron sludge due to the slow transformation of Fe^{3+} to Fe^{2+}, and the presence of residual Fe^{3+} ions in the treated wastewater, necessitating an additional separation step.[216]

To address these challenges, the combination of heterogeneous catalysts with these systems and the introduction of reductant can enhance the catalytic performance of homogeneous methods. Copper-aluminum containing systems were synthesized to accelerate MO degradation.[217] Heterogeneous systems offer the advantage of operating over a wide pH range. However, these approaches have limitations, including their cost, lengthy reaction times, and potential for secondary pollution. Several other methods, like the photo-Fenton process,[218] sono-Fenton process,[219] and electro-Fenton process,[220] have been designed to enhance hydroxyl radical generation and reduce H_2O_2 consumption. Ozone-based advanced oxidation is an affordable and easily operated process for MO degradation. To enhance oxidation efficiency, various catalysts, like ultrasonic and ultraviolet catalysts, are applied along with ozone. These catalysts generate hydroxyl radicals, improving the degradation process without producing secondary pollution such as chemical sludge.[221]

Therefore, in the presence of nanocatalysts, toxic MO are degraded into less harmful products, contributing to environmental preservation. The nanocatalysts are employed as nanofilters to treat MO present in industrial wastewater before their discharge into water bodies.

6. Conclusion and future directions

In summary, this thorough review sheds light on various approaches to synthesizing metal NPs and incorporating them into various supporting materials. Various approaches to these nanocatalytic systems are discussed for treating MO like oxidation processes, photocatalytic treatment, and chemical reduction. The catalytic degradation of MO follows a pseudo first-order kinetic model along with the Langmuir–Hinshelwood mechanism. The reaction environments influence the MO reduction/oxidation rate. Several major findings have emerged from this part of research, guiding future directions in this important area. One significant outcome is the improved efficiency of bimetallic nanoparticles in catalytic degradation reactions for MO compared to monometallic nanoparticles. This highlights the prominence of adapting nanoparticles in nanocomposite forms to increase catalytic effects, which appears a favorable area for more development in this field. Furthermore, the stabilization of MNPs can be achieved by various supporting materials like polymeric, organic, and inorganic materials which extend their lifespan during catalytic performance without losing their efficiency. An essential look of advancing strategies for reducing MO involves optimizing reaction conditions. Factors like Initial MO concentration, reductant concentration, temperature, and pH levels play crucial roles for the reduction reaction efficiency. Precise control and adjustment of these factors can greatly improve the whole efficiency of metallic nanoparticles as catalysts. Catalytic reduction approaches are notable for their rapid reduction rates as well as scalability which makes them suitable for different applications on large-scale. Conversely, photocatalytic reduction approaches hold potential nevertheless further refinement is also required to minimize the amount of photocatalyst, hence improving cost-effectiveness. Moreover, oxidation reactions like Fenton-oxidation and wet air oxidation reactions have demonstrated effectiveness in converting MO into less harmful substances with higher costs. These approaches remain viable choices for particular applications where treatment efficacy outweighs cost considerations. This review contributes to the growing body of knowledge directing us toward a more environmentally sustainable future.

Metal nanoparticles along with caping agent are the best materials for removal of pollutants from wastewater due to easy recycling ability as well as adsorption capacity. The adsorption capacity of polar parts of the capping agent facilitates the approach pollutant towards the surface of metal nanoparticles. The diffusion rate of different pollutants in composites is the available vacant space of research in this field. This study helps to find a most suitable composite for removal of pollutants from wastewater and the composite has low cost, easy recycling ability, rapid removal of pollutants.

Abbreviations

NIPMAM	*N*-Isopropylmethacrylamide
NIPAM	*N*-Isopropylacrylamide
NPs	Nanoparticles
MNPs	Metal nanoparticles
IMNPs	Inorganic metal nanoparticles
MB	Methylene blue
CR	Congo red
4NP	4-Nitrophenol
MO	Methyl orange
RhB	Rhodamine-B
GO	Graphene oxide
RGO	Reduced graphene oxide
WAO	Wet air oxidation
ER	Eley Ridel
LH	Langmuir–Hinshelwood
PAL	Polyacrylate
NM	*N*-Isopropylmethacrylamide-methacrylic acid
PDA	Polydopamine
E_a	Activation energy
PVP	Polyvinylpyrrolidone
P(EG)	Poly(ethylene glycol)
P(VA)	Poly(vinyl alcohol)
RM	Redox mediator (RM),
ZIMFs	Zeolitic imidazolate frameworks
SRB	Stimuli responsive behavior
FTIR	Fourier transformed infrared spectroscopy
HDR	Hydrodynamic radius
TEM	Transmission electron microscopy
LCST	Lower critical solution temperature
MOFs	Metal–organic frameworks
MS	Mesoporous silica (MS)
AC	Activated carbon
APS	Ammonium persulfate
C	Carbon
Ag	Silver
Au	Gold
N	Nitrogen

CN	Carbon nitride
SPR	Surface plasmon resonance
UV-vis	UV/visible spectroscopy
VPTT	Volume phase transition temperature
HDD	Hydrodynamic diameter
P(EI)	Poly(ethyleneimine)

Conflicts of interest

There is no conflict of interest.

Data availability

No primary research results, software has been included and no new data were generated or analysed as part of this review.

Acknowledgements

Muhammad Arif is thankful to University of Management and Technology, Lahore-54770, Pakistan.

References

1 V. Launay, A. Caron, G. Noirbent, D. Gigmes, F. Dumur and J. Lalevée, *Adv. Funct. Mater.*, 2021, **31**, 2006324.
2 T. Bujak, M. Zagórska-Dziok, A. Ziemlewska, Z. Nizioł-łukaszewska, K. Lal, T. Wasilewski and Z. Hordyjewicz-Baran, *Molecules*, 2022, **27**, 922.
3 W. Ding, H. Liu, S. Li, J. Remón, X. Pang and Z. Ding, *ACS Sustain. Chem. Eng.*, 2022, **10**, 17346–17354.
4 R. Karadag, *J. Nat. Fibers*, 2023, **20**, 2162187.
5 M. A. Al Fahad, R. Ahamed, T. Ahmed, N. Jahan, R. Mia, G. F. I. Toki, S. T. Mahmud and K. K. Niloy, *Renewable Dyes and Pigments*, 2024, pp. 165–175.
6 P. Amchova, F. Siska and J. Ruda-Kucerova, *Toxics*, 2024, **12**, 466.
7 M. Farhan Hanafi and N. Sapawe, *Mater. Today Proc.*, 2020, **31**, A141–A150.
8 E. Wargala, M. Sławska, A. Zalewska and M. Toporowska, *Women*, 2021, **1**, 223–237.
9 M. Ismail, K. Akhtar, M. I. Khan, T. Kamal, M. A. Khan, A. M. Asiri, J. Seo and S. B. Khan, *Curr. Pharm. Des.*, 2019, **25**, 3645–3663.
10 Y. A. Seulieman, N. J. Aziz al-khafaji, A. E. Abdulwahab, I. M. Saadoon and H. Lazim, *J. Forensic Leg. Med.*, 2024, **105**, 102712.
11 H. Kolya and C. W. Kang, *Toxics*, 2024, **12**, 111.
12 S. Sudarshan, S. Harikrishnan, G. RathiBhuvaneswari, V. Alamelu, S. Aanand, A. Rajasekar and M. Govarthanan, *J. Appl. Microbiol.*, 2023, **134**, 1–23.
13 A. Jankowska, A. Ejsmont, A. Galarda and J. Goscianska, *Sustainable Materials for Sensing and Remediation of Noxious Pollutants*, 2022, pp. 15–37.
14 M. Yasasve, M. Manjusha, D. Manojj, N. M. Hariharan, P. Sai Preethi, P. Asaithambi, N. Karmegam and M. Saravanan, *Chemosphere*, 2022, **307**, 136017.
15 M. Kert and J. Skoko, *Polymers*, 2023, **15**, 1783.
16 Q. V. Vo, B. T. Truong-Le, N. T. Hoa and A. Mechler, *J. Mol. Struct.*, 2025, **1323**, 140631.
17 H. Rahnama, S. M. Mazloomi, E. Berizi, A. Abbasi and Z. Gholami, *Food Sci. Nutr.*, 2022, **10**, 3781–3788.
18 A. Raina, S. Kaul and M. K. Dhar, *Food Control*, 2024, **155**, 110042.
19 V. Ashok, N. Agrawal, J. Esteve-Romero, D. Bose and N. P. Dubey, *Food Anal. Methods*, 2017, **10**, 269–276.
20 E. K. Essuman, E. Teye, R. G. Dadzie and L. K. Sam-Amoah, *Int. J. Food Sci.*, 2023, **2023**, 5337150.
21 R. Varghese and S. Ramamoorthy, *J. Verbraucherschutz Lebensmittelsicherh.*, 2023, **18**, 107–118.
22 M. Gebishu, B. Fikadu, B. Bekele, L. Tesfaye Jule, N. N and K. Ramaswamy, *Sci. Rep.*, 2022, **12**, 1–9.
23 L. Fu, Y. N. Bai, Y. Z. Lu, J. Ding, D. Zhou and R. J. Zeng, *J. Hazard. Mater.*, 2019, **364**, 264–271.
24 S. A. Gheni, M. M. Ali, G. C. Ta, H. J. Harbin and S. A. Awad, *ACS Chem. Health Saf.*, 2024, **31**, 8–21.
25 X. Jiang, C. Liu, Y. Zeng, G. Jiang, Y. Peng, S. Xu, Z. Wang and Z. Liu, *J. Phys. Chem. C*, 2025, **129**, 1485–1494.
26 T. A. Homdi, T. M. Fagieh, K. Akhtar, E. M. Bakhsh, A. H. Alhemadan and S. B. Khan, *Int. J. Biol. Macromol.*, 2024, **268**, 131558.
27 A. Ranjbari, J. Kim, J. Yu, J. Kim, M. Park, N. Kim, K. Demeestere and P. M. Heynderickx, *Catal. Today*, 2024, **427**, 114413.
28 I. Ahmad, H. Alothaid, M. M. Habibullah, T. H. Wani and S. Ikram, *J. Environ. Manage.*, 2024, **367**, 121795.
29 A. Shahzaib, Shaily, I. Ahmad, M. A. Hashmi, M. A. Khan and N. Nishat, *Catal. Lett.*, 2024, **154**, 1567–1578.
30 O. Ouled Ltaief, S. Fourmentin, S. Siffert and M. Benzina, *React. Kinet., Mech. Catal.*, 2024, **137**, 547–570.
31 N. Ahmad, M. R. Khan, K. S. Velu and S. Mohandoss, *Mater. Chem. Phys.*, 2025, **340**, 130819.
32 A. S. Abdulhameed, R. H. Al Omari, A. Omari, S. Abdullah, A. A. Al-Masud, M. Abualhaija and S. Algburi, *J. Polym. Environ.*, 2024, **33**, 1086–1105.
33 S. Bawazeer, *Heliyon*, 2025, **11**, e41226.
34 F. M. Aldosari, A. F. El-kott, A. S. Alshehri, M. A. AlShehri, E. H. Ibrahim, S. Negm, B. Karmakar, M. A. Salem and M. H. Helal, *J. Inorg. Organomet. Polym. Mater.*, 2025, 1–15.
35 Y. Xie and X. L. Xia, *Mater. Lett.*, 2025, **385**, 138164.
36 R. Aslam, S. R. Khan, S. Ali, S. Jamil, T. Kamal, S. Noreen, A. Raza, M. Fatima, A. Naeem and M. J. Latif, *J. Chem. Technol. Biotechnol.*, 2025, **100**, 873–882.
37 K. Nithya, N. Anbuselvan, R. Anbarasan, V. S. Vairathevar, S. Vasantha, D. Suresh and A. J. Amali, *Chempluschem*, 2025, **90**, e202400441.
38 S. Xue, P. Lin, Y. Pang, Z. Li, M. Zhou, X. Qiu and H. Lou, *Int. J. Biol. Macromol.*, 2024, **273**, 132899.
39 M. Sahin and I. H. Gubbuk, *React. Kinet. Mech. Catal.*, 2022, **135**, 999–1010.
40 K. Memon, R. Memon, A. Khalid, B. S. Al-Anzi, S. Uddin, S. T. H. Sherazi, A. Chandio, F. N. Talpur, A. A. Latif and I. Liaqat, *RSC Adv.*, 2023, **13**, 29270–29282.

41 P. D. Sarvalkar, A. P. Tibe, S. S. Kamble, O. S. Karvekar, S. B. Teli, P. S. Powar, D. N. Kurhe, M. S. Nimbalkar, N. R. Prasad and K. K. K. Sharma, *Catal. Commun.*, 2024, **187**, 106897.
42 M. Kgatle, K. Sikhwivhilu, G. Ndlovu and N. Moloto, *Catalysts*, 2021, **11**, 428.
43 B. Akilandaeaswari and K. Muthu, *J. Taiwan Inst. Chem. Eng.*, 2021, **127**, 292–301.
44 T. Iqbal, H. Bilal, S. Afsheen, H. I. Rizvi, S. Kausar, R. M. Munir, H. A. El-Serehy and B. M. Al-Maswari, *Mater. Today Commun.*, 2025, **42**, 111250.
45 H. Qayyum, S. Hussain, W. Ahmed, A. N. Al-Ahmadi and A. H. Abdel-Aty, *J. Phys. Chem. Solids*, 2025, **196**, 112408.
46 K. Shanmugaraj, S. Bedoya, D. González-Vera, C. H. Campos, M. Mathivanan, M. Arivazhagan, P. Annamalai, V. M. Gowri and P. Thangavelu, *J. Water Process Eng.*, 2025, **71**, 107234.
47 K. Naseem, Z. H. Farooqi, R. Begum and A. Irfan, *J. Clean. Prod.*, 2018, **187**, 296–307.
48 M. Arif, H. Raza and T. Akhter, *RSC Adv.*, 2024, **14**, 38120–38134.
49 Z. H. Farooqi, M. W. Akram, R. Begum, W. Wu and A. Irfan, *J. Hazard. Mater.*, 2021, **402**, 123535.
50 J. Li, G. Xie, J. Jiang, Y. Liu, C. Chen, W. Li, J. Huang, X. Luo, M. Xu, Q. Zhang, M. Yang and Y. Su, *Nano Energy*, 2023, **108**, 108234.
51 J. Francis, N. P. Purayil, S. Edappadikkunnummal, P. L. Maria Linsha, C. Keloth and C. S. S. Sangeeth, *Opt. Mater.*, 2023, **146**, 114571.
52 N. S. Arunsankar, S. Devanesan, M. S. AlSalhi, M. Vimalan and S. Jeyaram, *J. Fluoresc.*, 2024, **35**, 1961–1968.
53 B. Bisht, P. Bhardwaj, M. Giri and S. Pant, *J. Fluoresc.*, 2021, **31**, 1787–1795.
54 S. Kumari Nisha, S. Sivakumar and S. Achutha, *Mater. Today Proc.*, 2021, **42**, 1008–1011.
55 S. S. Hemdan, A. Mansour and F. K. Ali, *J. Fluoresc.*, 2024, **34**, 675–689.
56 K. You, O. P. Kwon and D. Kim, *Bull. Korean Chem. Soc.*, 2023, **44**, 523–527.
57 K. Sivaranjani, R. Ariyamuthu, S. Devanesan, M. S. AlSalhi, M. Vimalan and S. Jeyaram, *J. Fluoresc.*, 2024, **35**, 1919–1926.
58 M. Arif, F. Tahir, A. Saeed, A. Mohyuddin and S. Nadeem, *Chem. Data Collect.*, 2022, **41**, 100943.
59 A. K. Ilunga, B. B. Mamba and T. T. I. Nkambule, *Appl. Organomet. Chem.*, 2021, **35**, e6050.
60 K. Aruna Kumari, G. Bhagavanth Reddy, V. Ramadevi and V. Mittepalli, *Inorg. Nano-Met. Chem.*, 2025, **55**, 421–430.
61 S. M. Ghoreishi and S. Mortazavi-Derazkola, *Heliyon*, 2025, **11**, e40104.
62 G. Lavanya, K. Anandaraj, K. Selvam, M. Gopu, T. Selvankumar, M. Govarthanan and P. Kumar, *Polym. Adv. Technol.*, 2024, **35**, e6383.
63 H. A. Bukhamsin, H. H. Hammud, C. Awada and T. Prakasam, *Catalysts*, 2024, **14**, 89.
64 A. Belhadri, B. Boukoussa, F. Benali, A. Mekki, A. Mokhtar, M. Hachemaoui, I. Ismail, J. Iqbal, S. P. Patole, I. Taha, R. Hamacha and M. Abboud, *J. Water Process Eng.*, 2025, **70**, 106954.
65 S. Jangra, A. Raza, B. Kumar, J. Sharma, S. Das, K. Pandey, Y. K. Mishra and M. S. Goyat, *Mater. Sci. Eng., B*, 2025, **311**, 117832.
66 M. F. Gebreaneniya, G. G. Berhe and T. Teklu, *Adv. Mater. Sci. Eng.*, 2024, **2024**, 9969064.
67 C. Chen, Z. Yan, Z. Ma, D. Ma, S. Xing, W. Li, J. Yang and Q. Han, *Chin. J. Chem. Eng.*, 2025, **77**, 144–155.
68 M. Qasim, K. Nadeem, M. Shahid, M. Z. Khan and A. Baqi, *Ceram. Int.*, 2025, **51**, 11467–11479.
69 M. Söyleyici Çergel, E. Demir and S. Kurtaran, *Indian J. Phys.*, 2024, **99**, 1289–1298.
70 A. Ekinci, Ö. Şahin and O. Baytar, *Process Saf. Environ. Prot.*, 2024, **187**, 644–651.
71 W. Xie, Y. Zhang, X. Yang, P. Yu and D. Ban, *Inorg. Chem. Commun.*, 2024, **162**, 112169.
72 S. H. Mousavi, M. Yaghoobi and F. Asjadi, *Sci. Rep.*, 2024, **14**, 1–20.
73 M. Hamieh, N. Tabaja, K. Chawraba, Z. Hamie, M. Hammoud, S. Tlais, T. Hamieh and J. Toufaily, *Molecules*, 2025, **30**, 1770.
74 T. Riaz, S. Nayyar, T. Shahzadi, M. Zaib, S. Shahid, S. Mansoor, M. Javed, S. Iqbal, M. M. Al-Anazy, E. B. Elkaeed, R. A. Pashameah, E. Alzahrani and A. E. Farouk, *Agronomy*, 2022, **12**, 2505.
75 M. Arif, H. Raza, S. M. Haroon, S. Ben Moussa, F. Tahir and A. Y. A. Alzahrani, *Int. J. Biol. Macromol.*, 2024, **270**, 132331.
76 F. R. Karaduman, B. Ö. Köksal, A. Ü. Metin and N. Horzum, *Macromol. Rapid Commun.*, 2025, **46**, 2401033.
77 S. Zhang, C. Lei and L. Song, *Ceram. Int.*, 2023, **49**, 26548–26557.
78 S. Saikia, M. Saikia, S. A. Khanam, S. Lee, Y. Bin Park, L. Saikia, G. Gogoi and K. K. Bania, *Mater. Adv.*, 2023, **4**, 6244–6258.
79 S. Hadaoui, G. Tran, A. Naitabdi and A. Courty, *Nanoscale*, 2025, **17**, 3277–3287.
80 Y. Ben Smida, O. Oyewo, S. Ramaila, L. Mavuru, R. Marzouki, D. C. Onwudiwe and A. H. Hamzaoui, *J. Inorg. Organomet. Polym. Mater.*, 2022, **32**, 4679–4693.
81 Y. Q. Dou, T. S. Deng, Q. Zhang, X. Zhao, J. Liu and Z. Cheng, *J. Mater. Sci.*, 2023, **58**, 7583–7593.
82 Q. Wu, P. Zhang, D. H. Kuo, B. Wu, A. B. Abdeta, Z. Su, L. Chen, O. A. Zelekew, J. Lin and X. Chen, *J. Environ. Chem. Eng.*, 2023, **11**, 109974.
83 C. L. Song, Z. Li, Y. N. Zhang, G. Zhang and Y. W. Yang, *Supramol. Mater.*, 2023, **2**, 100035.
84 A. A. A. Zaid, L. M. Ahmed and R. K. Mohammad, *J. Nanostruct.*, 2023, **13**, 193–203.
85 A. H. Ajil, N. M. Ahmed, F. K. Yam, Z. U. Zango, I. A. Wadi, A. M. Binzowaimil, O. Aldaghri, K. H. Ibnaouf and H. Cabrera, *Appl. Sci.*, 2023, **13**, 11857.
86 K. Nagaraj, P. Thangamuniyandi, S. Kamalesu, M. Dixitkumar, A. K. Saini, S. K. Sharma, J. Naman, J. Priyanshi, C. Uthra, S. Lokhandwala, N. M. Parekh, S. Radha, S. Sakthinathan, T. W. Chiu and C. Karuppiah, *Inorg. Chem. Commun.*, 2023, **155**, 110985.

87 D. Khwannimit, R. Maungchang and P. Rattanakit, *Int. J. Environ. Anal. Chem.*, 2022, **102**, 5247–5263.
88 K. A. Tania, E. J. Das, M. Tahsin and M. A. R. Bhuiyan, *Biorem. J.*, 2024, DOI: 10.1080/10889868.2024.2381015.
89 N. E. A. El-Naggar, R. A. Hamouda, A. A. Saddiq and M. H. Alkinani, *Sci. Rep.*, 2021, **11**, 1–19.
90 T. Fan, X. Liu, H. Sheng, M. Ma, X. Chen, Y. Yue, J. Sun and Y. K. Kalkhajeh, *J. Hazard. Mater.*, 2024, **478**, 135362.
91 C. Amudha and M. Santhi, *Biomass Convers. Biorefin.*, 2025, 1–13.
92 M. Arif, H. Raza, F. Tahir, S. Ben Moussa, S. M. Haroon, A. Y. Abdullah Alzahrani and T. Akhter, *J. Mol. Liq.*, 2024, **416**, 126516.
93 D. Guo, M. Zhang, Y. Gao, A. Wang, W. Wang, Z. Song and Y. Mao, *Environ. Dev. Sustain.*, 2025, 1–20.
94 M. Elumalai, A. Baskaran, V. sadaiyandi, S. G. Ramaraj, N. kumar, P. C. Karthika and N. Rajendiran, *Chemosphere*, 2024, **362**, 142748.
95 M. S. J. Khan, L. M. Sidek, T. Kamal, A. M. Asiri, S. B. Khan, H. Basri, M. H. Zawawi and A. N. Ahmed, *Int. J. Biol. Macromol.*, 2024, **257**, 128544.
96 M. Arif, M. Shahid, A. Irfan, X. Wang, H. Noor, Z. H. Farooqi and R. Begum, *Inorg. Chem. Commun.*, 2022, **144**, 109870.
97 Z. Yang, M. Shahriari, Y. Liang, B. Karmakar, A. F. El-kott, M. A. AlShehri, S. Negm and W. Eltantawy, *J. Sci. Adv. Mater. Devices*, 2024, **9**, 100709.
98 B. Chen, L. Fan, C. Li, L. Xia, K. Wang, J. Wang, D. Pang, Z. Zhu and P. Ma, *Analyst*, 2024, **149**, 4283–4294.
99 M. Tanaka, Y. Kiriki, N. Kiyohara, M. Hayashi, A. Tamang, T. Nakamura, M. Vacha, Y. Choi, J. Choi, W. Yoshida, K. Critchley, S. D. Evans and M. Okochi, *ACS Appl. Nano Mater.*, 2024, **7**, 11258–11266.
100 M. Ridwansyah, O. U. R. Abid, W. Rehman, F. Ilfan, Hamzah, S. Khan, K. D. Badshah, N. Ahmed, J. Ahmed, A. Ali and K. Mehdi, *Curr. Res. Green Sustainable Chem.*, 2024, **9**, 100434.
101 M. Şahin, Y. Arslan, F. Tomul, B. Yıldırım and H. Genç, *React. Kinet., Mech. Catal.*, 2022, **135**, 3303–3315.
102 R. Rajasekar, R. Thanasamy, M. Samuel, T. N. J. I. Edison and N. Raman, *Biochem. Eng. J.*, 2022, **187**, 108447.
103 N. Garg, S. Bera, L. Rastogi, A. Ballal and M. V. Balaramakrishna, *Spectrochim. Acta, Part A*, 2020, **232**, 118126.
104 S. Nangan, A. L. MariaJoseph, P. Pattananuwat, S. Rajendran, S. A. Alharbi, J. R. Gnanapragasam and M. Okhawilai, *J. Taiwan Inst. Chem. Eng.*, 2025, **166**, 105487.
105 J. I. Ike, A. K. Babayemi, T. C. Egbosiuba, C. G. Jin, S. Mustapha, A. S. Yusuff, V. K. Yadav and C. A. Igwegbe, *ACS Appl. Eng. Mater.*, 2024, **2**, 1031–1046.
106 Q. Zeng, H. Lin, Y. Qu, Z. Huang, N. Kong, L. Han, C. Chen, B. Li, J. Teng, Y. Xu and L. Shen, *J. Clean. Prod.*, 2023, **415**, 137910.
107 K. Seku, S. S. Hussaini, M. Hussain, M. A. Siddiqui, N. Golla, D. Ravinder and B. Reddy G, *Phys. E*, 2022, **140**, 115169.
108 K. Naseem, F. Ali, M. H. Tahir, M. Afaq, H. M. Yasir, K. Ahmed, A. muteb Aljuwayid and M. A. Habila, *J. Mol. Struct.*, 2022, **1262**, 132996.
109 M. Majadleh, T. Shahwan, R. B. Ahmed and M. Anjass, *Water Resour. Ind.*, 2022, **28**, 100189.
110 O. Moradi, A. Pudineh and S. Sedaghat, *Food Chem. Toxicol.*, 2022, **169**, 113412.
111 C. Alex Mbachu, A. Kamoru Babayemi, T. Chinedu Egbosiuba, J. Ifeanyichukwu Ike, I. Jacinta Ani and S. Mustapha, *Results Eng.*, 2023, **19**, 101198.
112 L. N. Ndlovu, K. I. Malatjie, C. Donga, A. K. Mishra, E. N. Nxumalo and S. B. Mishra, *J. Appl. Polym. Sci.*, 2023, **140**, e53270.
113 H. Tang, W. Zhang, Y. Meng, B. Xie, Z. Ni and S. Xia, *Mater. Res. Bull.*, 2021, **144**, 111497.
114 J. Ashraf, G. A. Khan, M. ul Ain, M. A. Ghanem, K. M. H. Mohammed and W. Ahmed, *Inorg. Chem. Commun.*, 2024, **169**, 113039.
115 L. Boubkr, A. K. Bhakta, Y. Snoussi, C. Moreira Da Silva, L. Michely, M. Jouini, S. Ammar and M. M. Chehimi, *Catalysts*, 2022, **12**, 1475.
116 T. T. H. Pham, X. H. Vu, N. D. Dien, T. T. Trang, N. Van Hao, N. D. Toan, N. Thi Ha Lien, T. S. Tien, T. T. K. Chi, N. T. Hien, P. M. Tan and D. T. Linh, *R. Soc. Open Sci.*, 2023, **10**, 221623.
117 M. Arif, F. Tahir, U. Fatima, R. Begum, Z. H. Farooqi, M. Shahid, T. Ahmad, M. Faizan, K. Naseem and Z. Ali, *Mater. Today Commun.*, 2022, 104700.
118 D. S. Idris, A. Roy, A. Malik, A. A. Khan, K. Sharma and A. Roy, *J. Inorg. Organomet. Polym. Mater.*, 2024, **35**, 594–606.
119 Á. D. J. Ruíz-Baltazar, *Ultrason. Sonochem.*, 2021, **73**, 105521.
120 V. S. D. Devulapalli, R. Kushwaha, E. Ovalle, H. D. Singh, P. Shekhar, D. Chakraborty, C. P. Vinod, R. Vaidhyanathan and E. Borguet, *ACS Appl. Nano Mater.*, 2022, **5**, 4744–4753.
121 M. Arif, *RSC Adv.*, 2023, **13**, 3008–3019.
122 R. Kumar Mandal, S. Ghosh and T. Pal Majumder, *Results Chem.*, 2023, **5**, 100788.
123 S. Hata, Y. Sakai, N. Tani, S. Kitano, H. Habazaki, A. Hirakawa, H. Tanaka, Y. Inomata, T. Murayama, M. Haruta, Y. Du, Y. Shiraishi and N. Toshima, *ACS Appl. Nano Mater.*, 2022, **5**, 16231–16241.
124 M. M. Ahmad, H. M. Kotb, S. Mushtaq, M. Waheed-Ur-rehman, C. M. Maghanga and M. W. Alam, *Crystals*, 2022, **12**, 72.
125 A. G. Ramu and D. Choi, *Sci. Rep.*, 2021, **11**, 1–13.
126 M. Arif, *J. Mol. Liq.*, 2023, **375**, 121346.
127 H. Kubendiran, D. Hui, M. Pulimi, N. Chandrasekaran, P. S. Murthy and A. Mukherjee, *Environ. Nanotechnol., Monit. Manage.*, 2021, **16**, 100561.
128 M. Köhler, N. Goodman Dlamini, A. Kotze Basson and V. Srirama Rajasekhar Pullabhotla, *Appl. Nanosci.*, 2023, **4**, 1–24.

129 A. B. Abdel-Aziz, N. Mohamed, R. M. El-taweel, H. Sh, A. I. Salim, K. Pal, I. S. Fahim, L. A. Said and A. G. Radwan, *Top. Catal.*, 2024, **67**, 103–122.
130 S. P. Minal and S. Prakash, *Bioscience Nanotechnology*, 2025, vol. 1, pp. 1–17.
131 R. Singaravelan, M. Shanmugam, A. A. Salam, P. Vasanthi, M. Magesh, D. Mani and Y. H. Ahn, *J. Inorg. Organomet. Polym. Mater.*, 2021, 1–14.
132 S. Ghosh, S. Roy, J. Naskar and R. K. Kole, *Sci. Rep.*, 2020, **10**(1), 1–14.
133 A. Riaz, B. S. Ibrar, K. Bibi, Z. Habib, S. Ikram, H. M. A. Shahzad, P. Zhao and Z. Zahra, *Sustainability*, 2024, **16**, 6958.
134 S. Agarwal, D. S. Kim, L. R. Nagappagari and Y. T. Yu, *Inorg. Chem. Commun.*, 2025, **180**, 114959.
135 H. Kanwal, F. Anwar, A. Tanvir, S. H. I. Abidi and M. W. Mumtaz, *RSC Adv.*, 2025, **15**, 13838–13856.
136 M. Arif, F. Tahir, T. Hussain, S. Alrokayan and T. Akhter, *RSC Adv.*, 2025, **15**, 8580–8593.
137 M. Arif, A. Rauf, H. Raza, S. Ben Moussa, S. M. Haroon, A. Y. A. Alzahrani and T. Akhter, *Int. J. Biol. Macromol.*, 2024, **275**, 133633.
138 S. Mandal, *Chem. Pap.*, 2025, **79**, 2105–2120.
139 K. Saravanan, M. Ilayaraja, P. Muthukrishnan, S. Ananthakrishnan, P. Ravichandiran and V. Jeevanantham, *J. Indian Chem. Soc.*, 2025, **102**, 101748.
140 M. Shahid, Z. H. Farooqi, R. Begum, M. Arif, M. Azam, A. Irfan and U. Farooq, *Z. Phys. Chem.*, 2022, **236**, 87–105.
141 A. N. Vu, N.-H. T. Le, T. M. T. Nguyen, U. N. Nguyen-Thai, K.-P. L. Nguyen and L. D. Vu, *Desalination Water Treat.*, 2025, **322**, 101218.
142 M. Gouda, M. M. Khalaf, M. F. Abou Taleb, M. A. Abdelaziz and H. M. Abd El-Lateef, *Fibers Polym.*, 2025, **26**, 2891–2909.
143 F. Zhou, D. He, G. Ren and H. Yarahmadi, *Sci. Rep.*, 2024, **14**, 1–14.
144 M. Faheem, T. Iqbal, S. Afsheen, A. Basit, R. M. Munir, M. I. Khan, A. M. Elgorban, H. A. AL-Shwaiman and H. I. Rizvi, *Opt. Mater.*, 2024, **157**, 116131.
145 H. Zhang, L. Zhao, C. Li, H. Liu, F. Yu and W. Wang, *New J. Chem.*, 2025, **49**, 5106–5116.
146 J. Yang, C. Wang, Z. Yu, T. Yu, B. Bai, G. Chen and Y. Tang, *Minerals*, 2025, **15**, 163.
147 L. Lv, Y. Li, J. Tang and F. Zhang, *Opt. Mater.*, 2025, **159**, 116600.
148 M. Bagherzadeh, M. H. C. Dastjerdi, J. Mokhtari, F. Abadian-Naeini and M. Mohsennia, *Clean. Eng. Technol.*, 2025, **11**, 100152.
149 Z. H. A. Al-khuder and F. F. Karam, *Results Chem.*, 2025, **15**, 102133.
150 B. M. Alotaibi, X. Chen, T. M. D. Alharbi, A. Heydari and C. L. Raston, *Chem.–Eur. J.*, 2025, **31**, e202403207.
151 Z. Y. Bi, S. Li, J. H. Dai, L. Yang, P. Liu, J. B. Xi and X. Peng, *Rare Met.*, 2025, **44**, 4679–4690.
152 J. León-Flores, J. L. Pérez-Mazariego, M. L. Marquina, M. Quintana-García, S. Tehuacanero-Cuapa, J. Ortega, C. Reyes-Damián and J. Arenas-Alatorre, *Mater. Sci. Eng., B*, 2025, **313**, 117881.
153 L. Zhang, Q. Zhang, C. Xiao, Y. Jia and J. Wu, *J. Water Proc. Eng.*, 2024, **66**, 106059.
154 A. A. Essawy, T. H. A. Hasanin, M. F. Hussein, E. F. El Agammy and A. E. N. I. Essawy, *Catalysts*, 2024, **14**, 466.
155 W. Li, Y. Liu, X. Pang, Y. Huang, Z. Dong, Q. Niu, Y. Xiong, S. Li, S. Li, L. Wang, H. Guo, S. Cui, S. Hu, Y. Li, T. Cha and L. Wang, *Nanomaterials*, 2025, **15**, 376.
156 I. C. Novoa-De León, J. Johny, S. Vázquez-Rodríguez, D. Avellaneda-Avellaneda, S. Shaji and S. Sepúlveda-Guzmán, *ACS Appl. Mater. Interfaces*, 2025, **17**, 17251–17259.
157 M. Sun and C. Wang, *Heliyon*, 2024, **10**, e24772.
158 A. A. El Foulani, S. Tarhouchi, I. Hammoudan, R. Saddik, A. Y. Abdullah Alzahrani and S. Tighadouini, *Results Surf. Interfaces*, 2025, **18**, 100455.
159 K. Montiel-Centeno, D. Barrera, F. García-Villén, S. Amaya-Roncancio, C. Viseras and K. Sapag, *Surf. Interfaces*, 2025, **56**, 105576.
160 M. Ulfa, I. U. Hasanah and I. Setiarini, *Bull. Chem. React. Eng. Catal.*, 2024, **19**, 470–479.
161 L. Wang, T. Li, L. Tao, H. Lei, P. Ma and J. Liu, *Process Saf. Environ. Prot.*, 2022, **158**, 79–86.
162 L. Sun, Z. Li, Z. Yuan, Y. Liu, S. Mei, F. Meng, X. Ouyang, Y. Xiong, K. Zhang and Z. Chen, *Appl. Sci.*, 2025, **15**, 3781.
163 H. Khojasteh, S. Mohammadi-Aghdam, K. Heydaryan, N. Sharifi, P. Aspoukeh, S. Khanahmadzadeh and B. Khezri, *J. Sol-Gel Sci. Technol.*, 2024, **111**, 362–380.
164 B. Boukoussa, K. R. Cherdouane, R. Zegai, A. Mokhtar, M. Hachemaoui, I. Issam, J. Iqbal, S. P. Patole, F. Z. Zeggai, R. Hamacha and M. Abboud, *Surf. Interfaces*, 2024, **44**, 103622.
165 S. Daffalla, N. Al Mousa, H. Ahmed, J. Alsuwailem, M. I. Almaghasla and M. R. El-Aassar, *C*, 2025, **11**, 27.
166 H. Nourolahi, S. Farhadi, R. Malakooti, M. Maleki and F. Mahmoudi, *CrystEngComm*, 2025, **27**, 1185–1205.
167 Y. Zhang, J. Xiang, H. Dong, D. Xie, X. Yuan, C. Deng and F. Wang, *Mater. Lett.*, 2025, **397**, 138832.
168 F. Hasani, J. B. Raoof, R. Ojani and M. Ghani, *Heliyon*, 2025, **11**, e42438.
169 A. Podborska and M. Luty-Błocho, *J. Mol. Struct.*, 2023, **1273**, 134312.
170 J. R. Deka, D. Saikia, T. H. Cheng, H. M. Kao and Y. C. Yang, *J. Environ. Chem. Eng.*, 2023, **11**, 109777.
171 S. Karimi, M. Gholinejad, R. Khezri, J. M. Sansano, C. Nájera and M. Yus, *RSC Adv.*, 2023, **13**, 8101–8113.
172 M. Arif, H. Raza, S. M. Haroon, K. Naseem, H. Majeed, F. Tahir, U. Fatima, S. M. Ibrahim and S. Ul Mahmood, *J. Mol. Liq.*, 2023, **392**, 123541.
173 M. Arif, M. Shahid, A. Irfan, J. Nisar, X. Wang, N. Batool, M. Ali, Z. H. Farooqi and R. Begum, *Z. Phys. Chem.*, 2022, **236**, 1219–1241.
174 M. Ali, S. Faizan, L. A. Shah, M. Ullah, R. Ullah, M. A. Ibrahim and H. M. Yoo, *J. Dispersion Sci. Technol.*, 2025, 1–12, DOI: 10.1080/01932691.2025.2461112.
175 I. Fatima, M. Ajmal, A. Naseem, A. Ali, F. Javed, M. A. Hashmi, K. Mahmood, M. Ahmad, F. Ullah and Z. Ahmad, *J. Appl. Polym. Sci.*, 2025, **142**, e56841.

176 A. Aziz, A. Khan, N. Ali, M. Ul-Islam, S. B. Khan, N. Azum, K. A. Alzahrani, M. A. Rub, I. Ullah and T. Kamal, *Inorg. Chem. Commun.*, 2025, **173**, 113854.
177 B. K. Singh, P. P. Pande, A. Chaurasiya, K. K. Dey and N. Kushwaha, *Int. J. Environ. Anal. Chem.*, 2024, 1–26, DOI: 10.1080/03067319.2024.2373358.
178 K. Zhou, Z. Zhang, J. Xue, J. Shang, D. Ding, W. Zhang, Z. Liu, F. Yan and N. Cheng, *Int. J. Biol. Macromol.*, 2022, **221**, 135–148.
179 J. Li, Q. Zhang, B. Chen, F. Li and C. Pang, *Int. J. Biol. Macromol.*, 2024, **276**, 133795.
180 M. Arif, A. Rauf, H. Raza, S. B. Moussa, S. M. Haroon, A. Y. A Alzahrani and T Akhter, *International Journal of Biological Macromolecules*, 2024, **275**, 133633.
181 S. Iqbal, N. Iqbal, S. Musaddiq, Z. H. Farooqi, M. A. Habila, S. M. Wabaidur and A. Iqbal, *Heliyon*, 2024, **10**, e25385.
182 H. Taghvaei, A. Bakhtyari, M. Rahimpour and M. Arshadi, *Colloids Surf., A*, 2025, **722**, 137271.
183 B. Ajitha, C. W. Ahn, P. V. K. Yadav and Y. A. K. Reddy, *J. Environ. Chem. Eng.*, 2021, **9**, 106291.
184 M. Ahmad, A. Haider, I. Shahzadi, A. Ul-Hamid, M. Imran, M. A. Khan, G. Ali, M. M. Soliman and M. Ikram, *J. Photochem. Photobiol., A*, 2025, **465**, 116365.
185 I. Sajid, A. Hassan, W. Wu, J. Zhang, K. S. Munawar, A. Irfan, A. R. Chaudhry, Z. H. Farooqi and R. Begum, *J. Mol. Liq.*, 2025, **433**, 127890.
186 A. Ahmad, P. G. Roy, A. Hassan, S. Zhou, M. Azam, M. A. Z. G. Sial, A. Irfan, F. Kanwal, R. Begum and Z. H. Farooqi, *Int. J. Biol. Macromol.*, 2024, **283**, 137965.
187 A. Dolatkhah, C. Dewani, M. Kazem-Rostami and L. D. Wilson, *Polymers*, 2024, **16**, 2500.
188 S. Chen and H. Liu, *Colloids Surf., A*, 2022, **635**, 128038.
189 L. Wang, N. Gao, F. Han, Y. Mao and J. Tian, *Sep. Purif. Technol.*, 2023, **326**, 124781.
190 Y. Wang, W. Feng, J. Li and Z. You, *Colloids Surf., A*, 2023, **670**, 131561.
191 M. Farooq, N. Rauf, S. A. Marwat, G. Shabbir, J. Ihsan and R. M. K. Mohamed, *Int. J. Biol. Macromol.*, 2024, **279**, 134879.
192 J. Aburabie, S. Mohammed, R. Straubinger and R. Hashaikeh, *J. Ind. Eng. Chem.*, 2025, **146**, 777–787.
193 R. H. Althomali, K. A. Alamry, A. M. Alosaimi and M. A. Hussein, *Polym. Polym. Compos.*, 2023, **31**, 09673911231159798.
194 Z. Bibi, M. Iqbal, M. Siddiq, A. Haleem, M. E. Khalifa, Z. I. Zaki, M. A. Amin and A. Ibrar, *J. Mol. Struct.*, 2025, **1333**, 141721.
195 Z. Joshani, H. Veisi, A. Kakanejadifard and B. Karmakar, *J. Polym. Environ.*, 2025, **33**, 1758–1777.
196 M. Arif, *J. Mol. Liq.*, 2024, **403**, 124869.
197 T. H. Bui, P. K. T. Pham, T. B. T. Truong, B. L. Do, T. G. T. Ho, P. A. Nguyen, H. P. Phan and T. Nguyen, *Arabian J. Sci. Eng.*, 2024, **49**, 7851–7861.
198 A. Gangal, N. Akhtar, P. Singh, S. Manori, M. Duseja, N. K. Sethiya and R. K. Shukla, *J. Mater. Sci.: Mater. Electron.*, 2025, **36**, 1–17.
199 S. Baghel, M. Khurana and P. Gupta, *Bull. Chem. React. Eng. Catal.*, 2025, **20**, 411–427.
200 T. S. Swathy, M. J. Antony and M. A. Jose, *Mater. Chem. Phys.*, 2025, **340**, 130788.
201 B. Jaleh, A. Sahraei, M. Eslamipanah, F. Seifikar, S. Azizian, S. Jalali, S. Enghardt, B. Kruppke, H. A. Khonakdar and M. B. Gawande, *Nano-Struct. Nano-Objects*, 2025, **42**, 101471.
202 M. Zaheer, M. J. Latif, S. Ali, S. Jamil, S. Bibi, S. R. Khan and M. A. Rehman, *Diam. Relat. Mater.*, 2025, **155**, 112320.
203 M. Khan, S. Ahmad, K. Akhtar and S. B. Khan, *J. Environ. Chem. Eng.*, 2025, **13**, 117432.
204 V. Thi Thu Nhu and V. T. Nguyen, *Nucl. Instrum. Methods Phys. Res., Sect. B*, 2025, **558**, 165560.
205 Y. Wang, J. Chen, S. Qin, X. Yang, Y. Ma and Y. Li, *Mater. Today Commun.*, 2025, **42**, 111204.
206 R. A. Putri, I. Safitri, K. Khoiriah, M. I. Sofyan, D. Deliza and S. Safni, *Moroc. J. Chem.*, 2025, **13**, 463–479.
207 S. Kobylinskyi, S. Sinelnikov, L. Kobrina, Y. Bardadym and S. Riabov, *RSC Adv.*, 2025, **15**, 17955–17971.
208 D. B. Adamu, E. Zereffa and T. A. Segne, *Chem. Pap.*, 2025, **79**, 2437–2452.
209 P. K. Prabhakaran, S. Balu, G. Sridharan, D. Ganapathy and A. K. Sundramoorthy, *Eng. Res. Express*, 2025, **7**, 015002.
210 M. Ahmad, A. Ghafoor, S. Haoran, U. Ali, M. Xianglong, A. Kamara, A. Nazir, Z. Jie, Z. Liu and Z. Yan, *J. Water Proc. Eng.*, 2025, **70**, 107001.
211 J. Wu, J. Yao, X. Zhu, D. Zuo, H. Zhang, S. Jiang and H. Li, *Adsorption*, 2025, **31**, 1–13.
212 K. Ameen, A. Javaid, M. Imran, A. Zulfiqar, S. M. Ibrahim, M. A. AlDamen, A. B. Ibragimov, M. Mateen and M. N. Akhtar, *J. Mol. Struct.*, 2025, **1341**, 142580.
213 G. R. Gagana, K. R. Pooja, G. Venkatesha, F. A. Alharthia, J. Manjanna, R. Harini, B. Nagaraju and G. Nagaraju, *J. Electron. Mater.*, 2025, **54**, 5312–5325.
214 R. Merdoud, F. Aoudjit, L. Mouni, V. Honavar, R. P. Moghadam, M. Palabathuni and V. V. Ranade, *ACS Omega*, 2025, **10**, 21377–21390.
215 T. Xia, M. Shi, Z. Liu and M. Yang, *Desalination Water Treat.*, 2024, **317**, 100152.
216 W. Bi, R. Du, H. Liu, P. Fu and Z. Li, *Water*, 2024, **50**, 166–178.
217 H. Asghar, V. Maurino and M. A. Iqbal, *Discov. Electrochem.*, 2025, **2**, 1–10.
218 J. Leichtweis, A. C. Ferreira Piazzi Fuhr, N. Welter, L. G. Ramírez Mérida and E. Carissimi, *Waste Biomass Valorization*, 2025, 1–13.
219 E. A. Serna-Galvis, J. Silva-Agredo, J. Lee, A. Echavarría-Isaza and R. A. Torres-Palma, *Molecules*, 2023, **28**, 1113.
220 F. R. Omi, M. Rastgar, M. Mohseni, U. Singh, W. Dilokekunakul, R. Keller, D. Wishart, M. Wessling, C. Davis Vecitis and M. Sadrzadeh, *Sep. Purif. Technol.*, 2025, **357**, 130083.
221 J. Dong, J. Yao, J. Tao, X. Shi and F. Wei, *Environ. Technol.*, 2023, **44**, 2512–2524.